Received: 15 January 2024 | Revised: 2 March 2024 | Accepted: 3 March 2024

DOI: 10.1002/sus2.193

REVIEW

Electrocatalytic synthesis of C–N coupling compounds from CO_2 and nitrogenous species

Zheng Zhang[1] | Danyang Li[1] | Yunchuan Tu[2] | Jiao Deng[3] | Huiting Bi[1] | Yongchao Yao[4] | Yan Wang[4] | Tingshuai Li[4] | Yongsong Luo[5] | Shengjun Sun[5] | Dongdong Zheng[5] | Sónia A. C. Carabineiro[6] | Zhou Chen[7] | Junjiang Zhu[1] | Xuping Sun[4,5]

[1]Hubei Key Laboratory of Biomass Fibers and Eco-Dyeing & Finishing, College of Chemistry and Chemical Engineering, Wuhan Textile University, Wuhan, Hubei, China

[2]School of Chemistry and Chemical Engineering, Chongqing University, Chongqing, China

[3]i-Lab, Vacuum Interconnected Nanotech Workstation (Nano-X), Suzhou Institute of Nano-Tech and Nano-Bionics, Chinese Academy of Sciences, Suzhou, Jiangsu, China

[4]Institute of Fundamental and Frontier Sciences, University of Electronic Science and Technology of China, Chengdu, Sichuan, China

[5]College of Chemistry, Chemical Engineering and Materials Science, Shandong Normal University, Jinan, Shandong, China

[6]LAQV-REQUIMTE, Department of Chemistry, NOVA School of Science and Technology, Universidade NOVA de Lisboa, 2829-516 Caparica, Portugal

[7]College of Materials, Xiamen University, Xiamen, Fujian, China

Correspondence

Zhou Chen, College of Materials, Xiamen University, Xiamen 361005, Fujian, China.
Email: zhouchen@xmu.edu.cn

Junjiang Zhu, Hubei Key Laboratory of Biomass Fibers and Eco-Dyeing & Finishing, College of Chemistry and Chemical Engineering, Wuhan Textile University, Wuhan 430200, Hubei, China.
Email: jjzhu@wtu.edu.cn

Xuping Sun, Institute of Fundamental and Frontier Sciences, University of Electronic Science and Technology of China, Chengdu 610054, Sichuan, China.
Email: xpsun@uestc.edu.cn

Funding information

National Natural Science Foundation of China, Grant/Award Numbers: 42277485, 21976141, 22272197, 22102184, 22102136, U22A20392; Natural Science Foundation of Hubei Province, Grant/Award Numbers: 2022CFB1001, 2021CFA034;

Abstract

The electrocatalytic synthesis of C–N coupling compounds from CO_2 and nitrogenous species not only offers an effective avenue to achieve carbon neutrality and reduce environmental pollution, but also establishes a route to synthesize valuable chemicals, such as urea, amide, and amine. This innovative approach expands the application range and product categories beyond simple carbonaceous species in electrocatalytic CO_2 reduction, which is becoming a rapidly advancing field. This review summarizes the research progress in electrocatalytic urea synthesis, using N_2, NO_2^-, and NO_3^- as nitrogenous species, and explores emerging trends in the electrosynthesis of amide and amine from CO_2 and nitrogen species. Additionally, the future opportunities in this field are highlighted, including electrosynthesis of amino acids and other compounds containing C–N bonds, anodic C–N coupling reactions beyond water oxidation, and the catalytic mechanism of corresponding reactions. This critical review also captures the insights aimed at accelerating the development of electrochemical C–N coupling reactions, confirming the superiority of this electrochemical method over the traditional techniques.

Department of Education of Hubei Province, Grant/Award Numbers: Q20221701, Q20221704; Joint Fund of Yulin University and Dalian National Laboratory for Clean Energy, Grant/Award Number: YLU-DNL Fund 2022008

KEYWORDS
C–N coupling, CO_2 reduction, electrocatalysis, nitrogenous species, reaction mechanism

1 | INTRODUCTION

Carbon dioxide (CO_2) emitted from fossil fuel utilization is a greenhouse gas, contributing to temperature increase and associated environmental and social challenges that deeply impact human life. Thus, there is an urgent need to capture[1–3] and utilize[4–9] CO_2 to mitigate and balance its concentration in the atmosphere. Amine scrubbing presently stands as a robust and proven technology for CO_2 capture,[10] paving the way for downstream CO_2 utilization on an industrial scale. Simultaneously, the rapid growth of power generation from renewable sources, such as solar energy and wind energy, highlights issues related to power storage due to the intermittent character of these energy sources. Electrocatalytic CO_2 reduction reaction (CO_2RR) emerges as an effective solution capable of not only storing power but also generating high-value-added C–C coupling products, such as ethylene, acetate, ethanol, and propanol.[11–13] Remarkably, membrane electrode assembly (MEA) cells demonstrate the potential for achieving hundreds of milliamperes per square centimeter at low cell voltage,[14–16] facilitating the practical application of electrocatalytic CO_2RR.

Despite substantial progress in the field of CO_2RR, the generated products still remain limited to single C or C–C coupling chemicals.[17–19] The exploration of novel pathways in electrocatalytic CO_2 reduction is becoming an essential pursuit within the broader realm of electrocatalysis, aiming to diversify the range of products originated from CO_2. Currently, the electrocatalytic synthesis of C–N coupling compounds from CO_2 and earth-abundant/waste nitrogenous species has been attracting significant attention within the scientific community.[20–23] Through these emerging methods, valuable C–N coupling species (such as urea, amine, and amide) have been successfully synthesized, thereby expanding the range of product categories beyond pure CO_2RR.[24–27] These organonitrogen compounds hold considerable importance for applications in agriculture, chemical synthesis, and pharmaceutical chemistry.

Among the available nitrogenous species, nitrogen (N_2) stands out as an appealing choice due to its abundance, constituting approximately 78% of the Earth's atmosphere. However, its catalytic activity is constrained by chemical inertness arising from the stable N≡N bond (941 kJ mol^{-1}) and relatively low solubility in aqueous electrolytes.[28–31] Additionally, nitric oxide (NO), a pollutant gas emitted from the combustion of fossil fuels in power vehicles, factories, and power plants, can be electrochemically reduced and used as nitrogenous species for the C–N coupling reaction, addressing environmental concerns while simultaneously producing high-value-added products.[32–35] Beyond gaseous nitrogenous species, water-soluble inorganic anions such as nitrite (NO_2^-) and nitrate (NO_3^-) have also been widely investigated in N-cycle electrocatalysis[36–38] and are considered as more attractive species for the synthesis of valuable organonitrogen compounds.[39–42] Figure 1 provides a concise overview of the electrocatalytic synthesis of C–N coupling compounds from CO_2 and various nitrogenous species facilitated by renewable energy.

In recent years, significant advances have been made in electrocatalytic C–N coupling reactions, with the publication of several important reviews dealing with the research progress in this field.[43–45] However, these reviews often concentrate on specific C–N coupling compounds or on particular nitrogenous species. In contrast, the present review provides a comprehensive summary of the research concerning the electrocatalytic synthesis of C–N coupling products from CO_2 and various nitrogen species, with a particular emphasis on the recent progress in urea, amide, and amine, synthesized through electrocatalytic C–N coupling reactions. The notable progress from urea to amide, and further, to amine is summarized, based on the reduction degree of the C atom adjacent to the amino group. For each C–N coupling compound, several representative studies are presented and the reaction mechanisms involving the corresponding catalysts are elucidated. Finally, some challenges and proposed research perspectives for future exploration in this field are highlighted, aiming to inspire and guide future research endeavors toward industrialization.

2 | ELECTROCATALYTIC C–N COUPLING TO UREA

Urea holds significant importance as the primary nitrogen fertilizer due to its crucial contributions to crop growth.[46] Additionally, urea is known for being nontoxic,

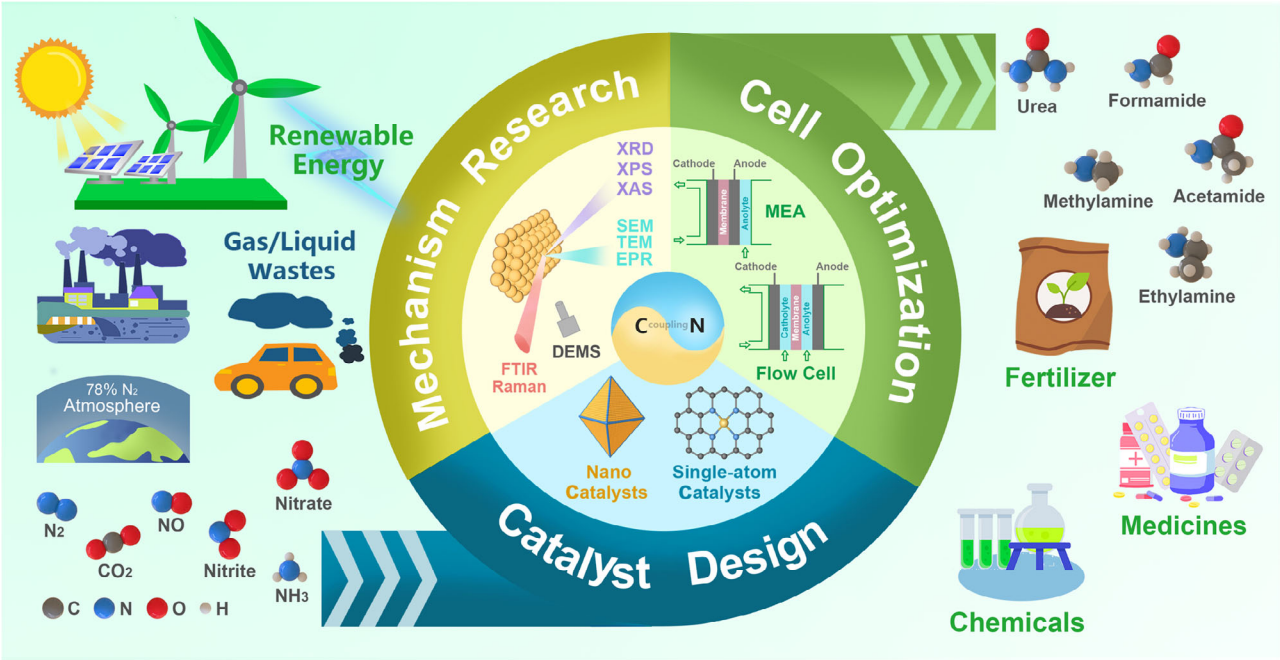

FIGURE 1 Schematic representation of the electrocatalytic synthesis of C–N coupling compounds.

stable, and having a high hydrogen mass concentration of 6.67%, making it a potential carrier for hydrogen transport and storage.[47,48] Presently, urea is usually generated through the reaction of CO_2 and NH_3, employing the Haber–Bosch process,[49,50] and 80% of the NH_3 produced globally is consumed for urea production.[51] However, the Haber–Bosch process generally runs at high temperature (400°C–650°C) and high pressure (200–400 bar), accounting for 1%–2% of the annual energy consumption of the whole world and contributing approximately to 1.4% of the global CO_2 emissions.[52,53] Consequently, there is a pressing need for an economical and environmentally friendly method enabling urea production directly under ambient conditions.

Electrosynthesis proves effective in converting feedstock to desired chemicals under mild conditions and using renewable energy. Unlike the Haber–Bosch process, which typically generates H_2 from water gas shift and steam–methane reforming, consuming energy resources and producing waste CO_2, electrosynthesis utilizes hydrogen derived from H_2O, the most abundant source on Earth's surface. Therefore, electrosynthesis emerges as a promising approach for urea synthesis.[54] Various nitrogen sources, however, trigger different reaction mechanisms, necessitating specific catalyst modulation. In this section, the state-of-the-art developments in electrocatalytic C–N coupling for urea synthesis are categorized and introduced, based on the nitrogen sources with different oxidation states. N_2 as the nitrogenous species is first introduced in this reaction. After that, recent research progress focused on nitrite is summarized, and followed by focusing on nitrate with the highest oxidation state for nitrogen.

2.1 | N_2 as the nitrogenous species

The activation of N_2 by electric energy enables catalytic reactions at lower temperatures and pressures, in contrast to the traditional Haber–Bosch process, which relies on thermal energy. However, the competitive reduction between CO_2 and N_2 presents challenges in enhancing the efficiency of C–N coupling, leading to undesirable urea selectivity. As shown in Table 1, recent advancements in this field address these challenges through careful design and synthesis of electrocatalysts.[66,67] Wang and coworkers conducted pioneering research on the electrocatalytic coreduction of CO_2 and N_2 to synthesize urea (Figure 2A).[55] They initially synthesized TiO_2 with oxygen vacancies (OVs), by treating original TiO_2 nanosheets under a reductive atmosphere, at high temperature, followed by coreduction of metal precursors, to fabricate PdCu alloy species on OV-rich TiO_2 (Figure 2B). The PdCu alloy demonstrates electronic interaction and corresponding charge transfer between Pd and Cu. When applied to the electrocatalytic coreduction of CO_2 and N_2, Pd_1Cu_1/TiO_2-400, having the highest vacancy concentration, exhibits the best performance for urea generation. Subsequently, a flow cell was used to enhance mass transport and improve catalytic activity. As expected, the formation rates for urea in flow cells

TABLE 1 Summary of urea electrosynthesis from CO_2 and N_2.

Catalyst	Electrolyte	Cell type	Potential (V vs. RHE)	FE (%)	Partial CD (mA cm^{-2})	Yield	Ref.
Pd_1Cu_1/TiO_2-400	0.1 M $KHCO_3$	Flow cell	−0.4	8.92	~0.16	3.36 mmol h^{-1} g^{-1}	55
$BiFeO_3/BiVO_4$	0.1 M $KHCO_3$	H cell	−0.4	17.18	~0.17	4.94 mmol h^{-1} g^{-1}	56
Bi-$BiVO_4$	0.1 M $KHCO_3$	H cell	−0.4	12.55	~0.23	5.91 mmol h^{-1} g^{-1}	57
$Ni_3(BO_3)_2$-150	0.1 M $KHCO_3$	H cell	−0.5	20.36	~0.31	9.70 mmol h^{-1} g^{-1}	58
CuPc NTs	0.1 M $KHCO_3$	H cell	−0.6	12.99	~0.12	143.47 μg h^{-1} mg^{-1}	59
Co-based MOF	0.1 M $KHCO_3$	H cell	−0.5	48.97	~0.49	14.47 mmol h^{-1} g^{-1}	60
InOOH-100	0.1 M $KHCO_3$	H cell	−0.4	20.97	~0.25	6.85 mmol h^{-1} g^{-1}	61
MoP-(101)	0.1 M $KHCO_3$	H cell	−0.35	36.5	~0.05	12.4 μg h^{-1} mg^{-1}	62
V_N-Cu_3N-300	0.1 M $KHCO_3$	H cell	−0.4	28.7	~0.11	81 μg h^{-1} cm^{-2}	63
Pd_1Cu_1–TiO_2	0.1 M $KHCO_3$	H cell	−0.5	22.54	~0.41	10 mmol h^{-1} g^{-1}	64
ZnMn–N,Cl	$KHCO_3$	H cell	−0.3	63.5	~0.19	4.13 mmol g^{-1} h^{-1}	65

Abbreviations: CD, current density; FE, Faradaic efficiency; MOF, metal-organic framework; NTs, nanotubes; RHE, reversible hydrogen electrode.

increased substantially, with the highest yield rate and Faradaic efficiency (FE) reaching 3.36 mmol g^{-1} h^{-1} and 8.92%, respectively, using 0.1 M $KHCO_3$ as electrolyte (Figure 2C). Temperature-programmed desorption results indicate that Pd_1Cu_1/TiO_2-400 has a stronger chemisorption affinity for N_2 and CO_2 individually and even exhibits favorable competition for the chemical coadsorption of CO_2 and N_2, contributing to the efficient urea production. The catalytic reaction mechanism study confirms that the coupling reaction proceeds through favorable C–N bond formation, which is a thermodynamically spontaneous reaction between *N N* intermediate and CO, followed by subsequent hydrogenation to generate urea.

Compared to metal nanoparticles, single-atom and dual-atom catalysts can not only maximize atomic utilization, but also exhibit high catalytic performance due to the presence of coordinatively unsaturated single atoms.[68–70] To discern which type is more effective for electrocatalytic urea synthesis, Wang and coworkers synthesized a Pd_1–TiO_2 single-atom catalyst and a Pd_1Cu_1–TiO_2 dual-atom catalyst using a vacancy-anchorage strategy (Figure 2D).[64] Aberration-corrected high-angle annular darkfield scanning transmission electron microscopy and Fourier transformed extended X-ray absorption fine structure (FT-EXAFS) spectra were carried out to demonstrate the coordination environment. When utilized for the electroreduction of CO_2 and N_2 in H-type cell, Pd_1Cu_1–TiO_2 exhibited much higher performance than Pd_1–TiO_2, achieving an urea formation rate of 166.67 mol_{urea} mol_{Pd}^{-1} h^{-1} and an FE of 22.54%, as seen in Figure 2E. Physicochemical characterizations, combined with theoretical modulations, suggest that the Pd_1Cu_1 site in Pd_1Cu_1–TiO_2 possesses a lower reaction energy barrier for C–N coupling, compared to Pd_1 in Pd_1–TiO_2 (Figure 2F). Recently, detailed calculations were conducted to explore the catalytic reaction of urea electrosynthesis from CO_2 and N_2 over N-doped graphene supporting bimetals.[71] The TiCo@NC catalyst exhibits an ultralow onset potential, where CO from CO_2 reduction preferentially engages in tilt-attack on *N_2 to form C–N bond. The catalytic activity has been promoted by modulating the electron transfer between the paired metallic sites.

Understanding the electrocatalytic C–N coupling process could inspire the rational design of single-atom and dual-atom catalysts for urea electrosynthesis from CO_2 and N_2. It is essential to use a well-structured electrocatalyst to elucidate the catalytic active sites and reaction mechanisms over electrocatalytic urea synthesis. Metal phthalocyanine can serve as a potential model electrocatalyst for studying the reaction mechanism, due to its specific molecular and atomic structures, as well as its excellent performances in the electrocatalytic reduction of both CO_2 and N_2.[72–75] Therefore, achieving green synthesis of urea by electrocatalytic reduction of CO_2 and N_2 can be accomplished using metal phthalocyanine as a catalyst. Ghorai and coworkers synthesized copper phthalocyanine nanotubes (CuPc NTs) using an ethylene glycol-assisted solvothermal technique.[59] The CuPc NTs exhibit several active sites, including metal Cu centers, pyrrolic-N3, pyrrolic-N2, and pyridinic-N1 (Figure 2G). In H-type cell, CuPc NTs exhibit a yield rate of 143.47 μg h^{-1} mg_{cat}^{-1} and an FE of 12.99% in 0.1 M $KHCO_3$ electrolyte (Figure 2H). Mechanism studies reveal that urea is synthesized via two active sites on CuPc, namely, pyridinic-N1 for N_2 reduction and Cu sites for CO_2 reduction (Figure 2I). The efficient CuPc NTs offer a new direction for the effective design over multiple metal-N sites for urea synthesis.

Recently, Wang and coworkers fabricated diatomic metal-N electrocatalysts through pyrolyzing the metal ion-coordinated polymers.[65] As the coordination environment

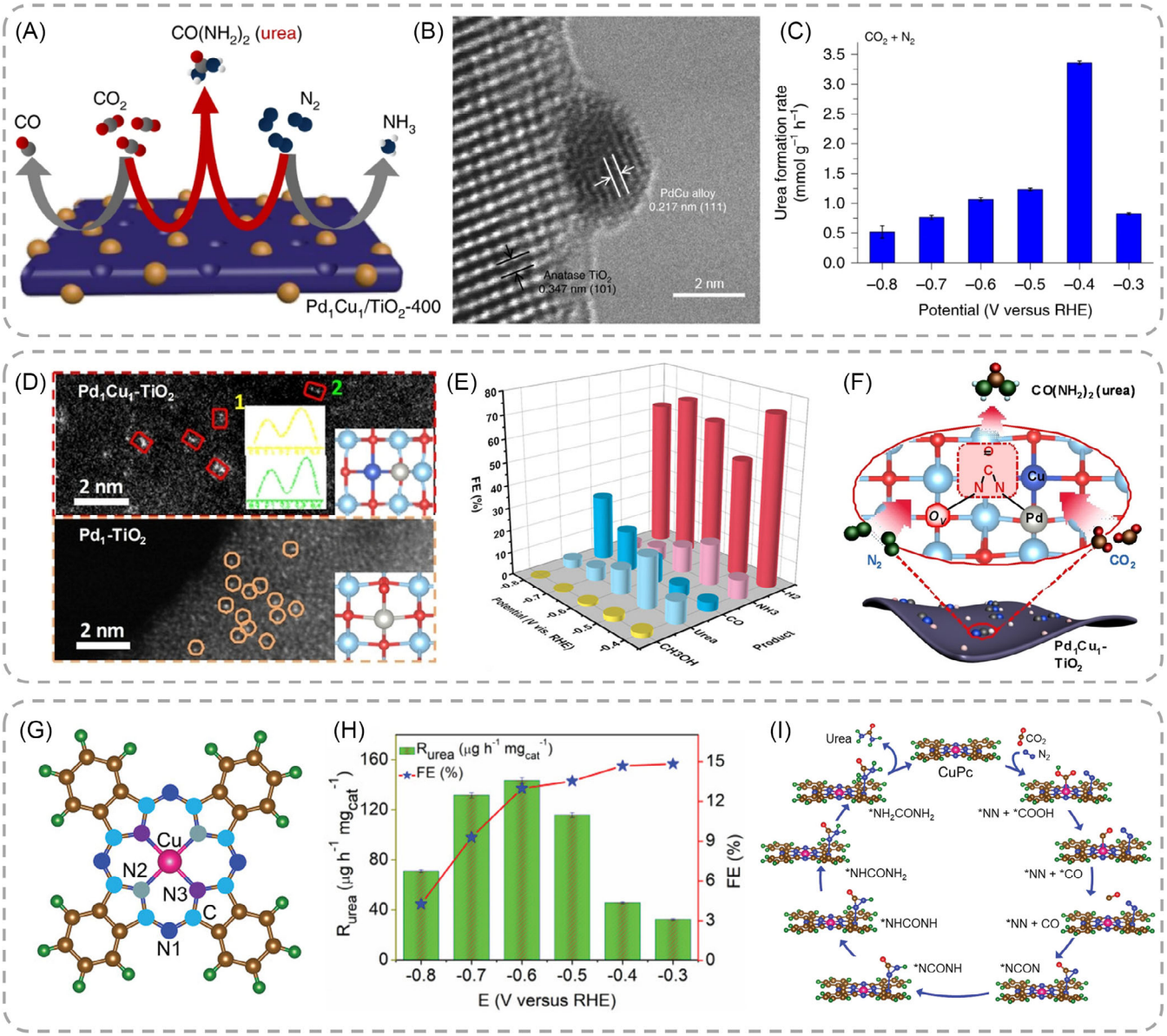

FIGURE 2 (A) Schematic illustration of Pd_1Cu_1/TiO_2-400 for the electrocatalytic reduction of CO_2 and N_2, (B) corresponding transmission electron microscopy (TEM) image, and (C) catalytic performance.[55] (D) High-angle annular dark-field scanning transmission electron microscopy (HAADF-STEM) images and the corresponding atomic structure (insets) of dual-atom Pd_1Cu_1–TiO_2 and single-atom Pd_1–TiO_2. (E) Catalytic performance over Pd_1Cu_1–TiO_2 and (F) corresponding schematic illustration.[64] (G) Molecular structure of CuPc and possible active sites, (H) corresponding catalytic performance, and (I) reaction mechanism.[59]

can help to tune the electronic structure and promote the catalytic progress, optimized Cl^- coordination on metal sites was achieved on ZnMn–N electrocatalysts through a hydrothermal method in diluted hydrochloric acid. The ZnMn–N,Cl catalyst exhibits an enhanced urea FE of 28.7% with a 4.0 mmol g^{-1} h^{-1} yield rate, while the ZnMn–N achieves only 15.0% FE with a 1.52 mmol g^{-1} h^{-1} yield rate. Negligible amounts of ammonia and hydrazine over ZnMn–N and ZnMn–N,Cl suggest that urea is the exclusive N-containing product with almost 100% N atom selectivity. Interestingly, the prepoisoning by CO on ZnMn–N,Cl significantly improves the urea FE to 63.5% without attenuating the urea yield rate, indicating that CO prepoisoning is an effective strategy to eliminate the side reactions. Mechanistic studies reveal that CO species insert into the side-on absorbed N_2 molecule, leading to rupture of the N–N bond and formation of *NCON* species. The one-step C–N coupling on diatomic electrocatalysts is the intrinsic factor accounting for approximately 100% N atom selectivity to urea, providing an important reference for unveiling mechanisms and designing catalysts.

In addition to the methods mentioned above for designing electrocatalysts, such as transitioning from bulk nanoparticles to single-atom and dual-atom materials and further to well-structured molecular catalysts for the electrocatalytic coreduction of N_2 and CO_2, other effective strategies involve designing p–n heterojunctions,[56] Mott–Schottky heterostructures,[57] frustrated Lewis pairs (FLPs),[58,61] and host–guest molecular interactions.[60] Zhang and coworkers constructed p–n heterojunction electrocatalysts for urea synthesis, using p-type $BiFeO_3$ and n-type $BiVO_4$ perovskite oxides as components. The $BiFeO_3/BiVO_4$ hybrids create a built-in electric field that accelerates the repartition of local charge, generating electrophilic and nucleophilic regions that help to promote the adsorption and activation of N_2 and CO_2.[56] Consequently, the $BiFeO_3/BiVO_4$ heterojunction achieves an yield rate of 4.94 mmol h^{-1} g^{-1} with an FE of 17.18% in 0.1 M $KHCO_3$ electrolyte. A comprehensive analysis demonstrates that the p–n heterojunction electrocatalyst within local charge redistribution can efficiently suppress CO poisoning and *NNH intermediate formation for ammonia generation, thus promoting C–N coupling between *N N* and CO to form *NCON* intermediate for urea production.

Apart from the p–n heterojunctions catalysts, Mott–Schottky structures, consisting of a metal–semiconductor heterojunction, were also reported as potential catalysts for the coreduction of CO_2 and N_2.[76] As a proof-of-concept catalyst, Bi–$BiVO_4$ hybrids have been prepared by the $NaBH_4$ reduction method, ensuring spontaneous electron transfer from $BiVO_4$ to Bi (Figure 3A).[57] The observed lattice spacings of 0.312 and 0.327 nm in transmission electron microscopy (TEM) correspond to the (130) crystal plane of $BiVO_4$ and the (012) crystal plane of Bi, respectively (Figure 3B). Mott–Schottky tests have been used to prove the electron transfer in Bi–$BiVO_4$ composites, showing that the $BiVO_4$ sample exhibits a positive slope in the Mott–Schottky curve, reflecting classical n-type semiconductor traits. Thus, combining with metallic Bi to form the Mott–Schottky structure, electrons transfer from $BiVO_4$ to Bi to form a special space-charge region. The synthesized Bi–$BiVO_4$ composites can realize urea yield rate of 5.91 mmol h^{-1} g^{-1} and an FE of 12.55% (Figure 3C). Mechanistic studies reveal that CO_2 and N_2 molecules are separately adsorbed on the generated nucleophilic/electrophilic regions due to the charge transfer at the Mott–Schottky composites. The generated CO will then attack *N_2 to form *NCON* via a thermodynamically favorable C–N coupling process, followed by a multistep proton-coupled electron transfer process for urea generation (Figure 3D). Therefore, the modulation of the space-charge region is also useful for fabricating high-performance electrocatalysts for urea electrosynthesis.

In addition, FLPs have also been developed for urea electrosynthesis. They consist of sterically hindered Lewis acids and Lewis bases, preventing bond formation. This unique characteristic provides the ability to chemisorb and activate two gas molecules simultaneously, at both the acid site and base site. As the proof-of-concept catalyst, the coordination unsaturated metal species can act as Lewis acid sites to chemisorb and activate N_2, and the hydroxyls as Lewis base sites to chemisorb and activate CO_2. For example, Zhang and coworkers have synthesized $Ni_3(BO_3)_2$ nanocrystals (NCs) (Figure 3E).[58] The subsequent annealing treatment helps cleaving the Ni–OH bonds and generate unsaturated Ni sites adjacent to hydroxyl groups (step 1). The amount and ratio of Ni–OH bonds and unsaturated Ni sites are modulated by the calcination temperature. The formed FLPs promote CO_2 chemisorption via orbital interactions, capturing C atoms of CO_2 on Lewis base sites (step 2). After that, the Lewis acid and Lewis base sites work cooperatively to activate the adsorbed CO_2, promoting the formation of *CO intermediates (step 3). When N_2 molecular is activated to *N N* on the FLP active sites by a side-on adsorption configuration (step 4), the spontaneous coupling reaction between *N N* and CO generates the *NCON* intermediate via a "s orbital carbonylation" strategy (step 5). After the subsequent hydrogenation steps (step 6), an urea molecule is produced and released from the FLPs (step 7).

Similarly, highly efficient InOOH NCs, owning In sites with electron-deficient Lewis acids and In–OH with electron-rich Lewis bases, have been investigated as the FLPs. They not only achieve the effect of chemisorbing N_2 and CO_2 through electronic interaction, but also promote the orbital-matched reaction intermediates *N N* and CO, leading to the C–N coupling progress for *NCON* generation. Accordingly, the InOOH FLPs achieve an urea yield rate of 6.85 mmol h^{-1} g^{-1} with an FE of 20.97%.[61] The concept of FLPs highlights the critical factors accounting for urea electrosynthesis and opens an avenue to develop novel electrocatalysts for coreduction of CO_2 and N_2.

2.2 | NO_2^- as the nitrogenous species

Electrocatalytic NO_2^- reduction is an applicable method for wastewater treatment and value-added chemical synthesis.[77] It is an attractive reaction for urea generation from NO_2^- and CO_2 coreduction, as two kinds of wastes can be recycled. Compared with gaseous N_2, the relatively high solubility in aqueous electrolyte for NO_2^- can enhance the reaction rate for large-scale applications. Furuya and coworkers first carried out this reaction for urea synthesis through a Cu-loaded gas diffusion layer

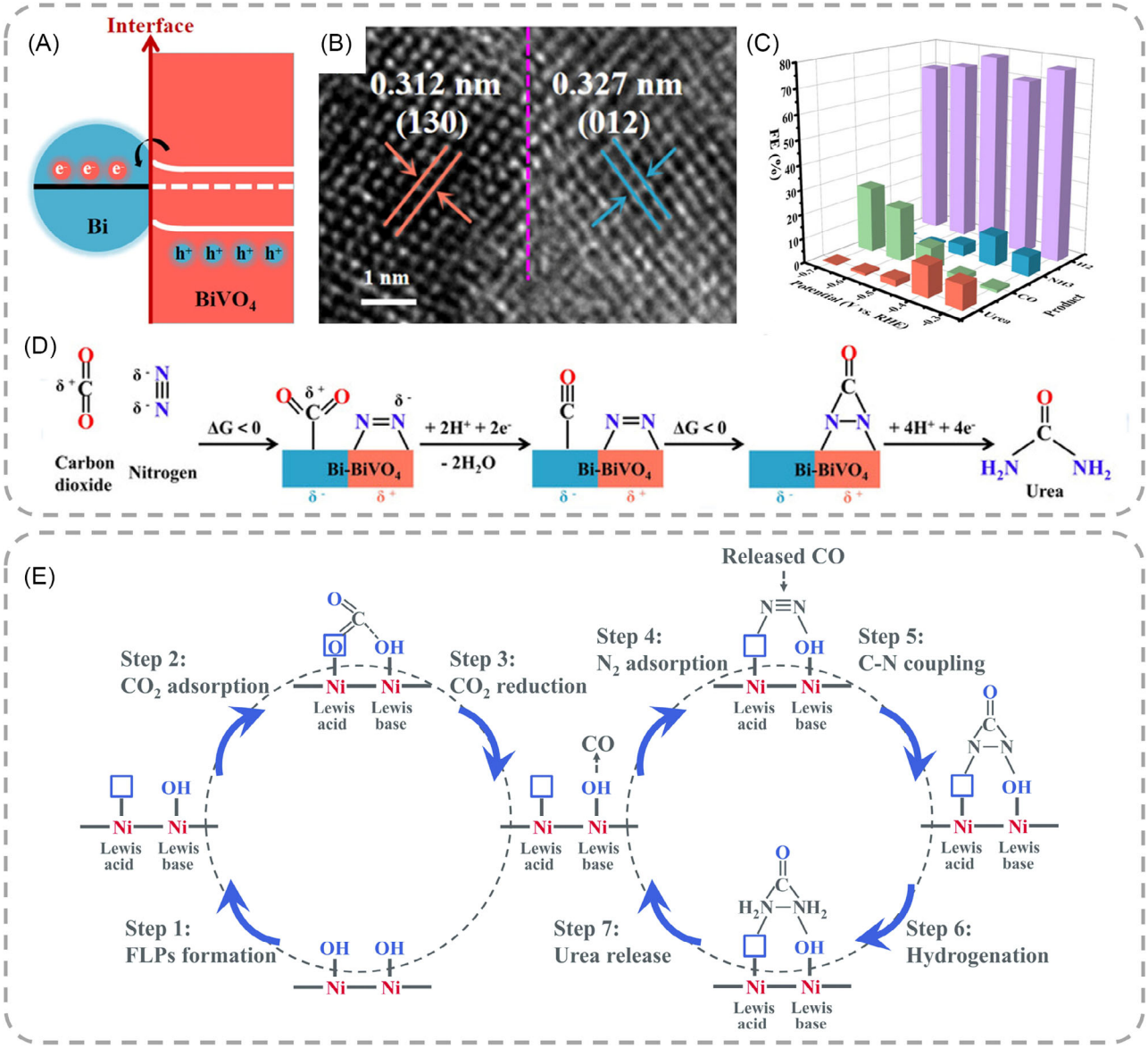

FIGURE 3 (A) Schematic illustration of the charge transfer in hybrid Bi–$BiVO_4$ with a Mott–Schottky heterostructure. (B) Corresponding transmission electron microscopy (TEM) image, (C) catalytic performance, and (D) reaction mechanism depiction of electrocatalytic urea synthesis.[57] (E) Schematic illustration of the electrocatalytic reduction of CO_2 and N_2 to urea via frustrated Lewis pairs (FLPs) on $Ni_3(BO_3)_2$-150 catalyst.[58]

in 1995.[78] Currently, with the significant advancement in electrosynthesis technology, the electrocatalytic coreduction of NO_2^- and CO_2 for urea production is currently being employed to achieve high catalytic efficiency. For instance, Zheng and coworkers synthesized OV-abundant anatase TiO_2 NTs with low-valence Cu dopants (Cu–TiO_2).[39] The high-density OVs in anatase TiO_2 are useful for reducing NO_2^- to NH_2* intermediate, while the low-valence Cu dopants provide major active sites for reducing CO_2 to CO* intermediate. Thereafter, the NH_2* and CO* intermediates, in close proximity, couple with each other to form urea via C N bonds. Cu–TiO_2 can enable a high urea yield rate of 20.8 μmol h^{-1}, with 43.1% FE. In addition, Shao and coworkers reported Te-doped Pd nanocrystals (Te–Pd NCs) for synthesizing urea, achieving a 12.2% FE and 88.7% N atom efficiency.[79] Mechanistic studies show that the synergetic effect between Te and Pd significantly promotes CO_2 and NO_2^- reduction to *CO and *NH_2, followed by the coupling step between *CO and *NH_2, leading to urea formation. Recently, Wang and coworkers synthesized ultrathin AuCu alloy nanowires possessing a Boerdijk–Coxeter structure trait for the electrosynthesis of urea.[40] The abundant defects in catalyst and AuCu bimetallic alloy composites provide rich active sites, which can help to achieve a high urea yield rate of 3889.6 μg h^{-1} mg_{cat}^{-1} with an FE of 24.7%.

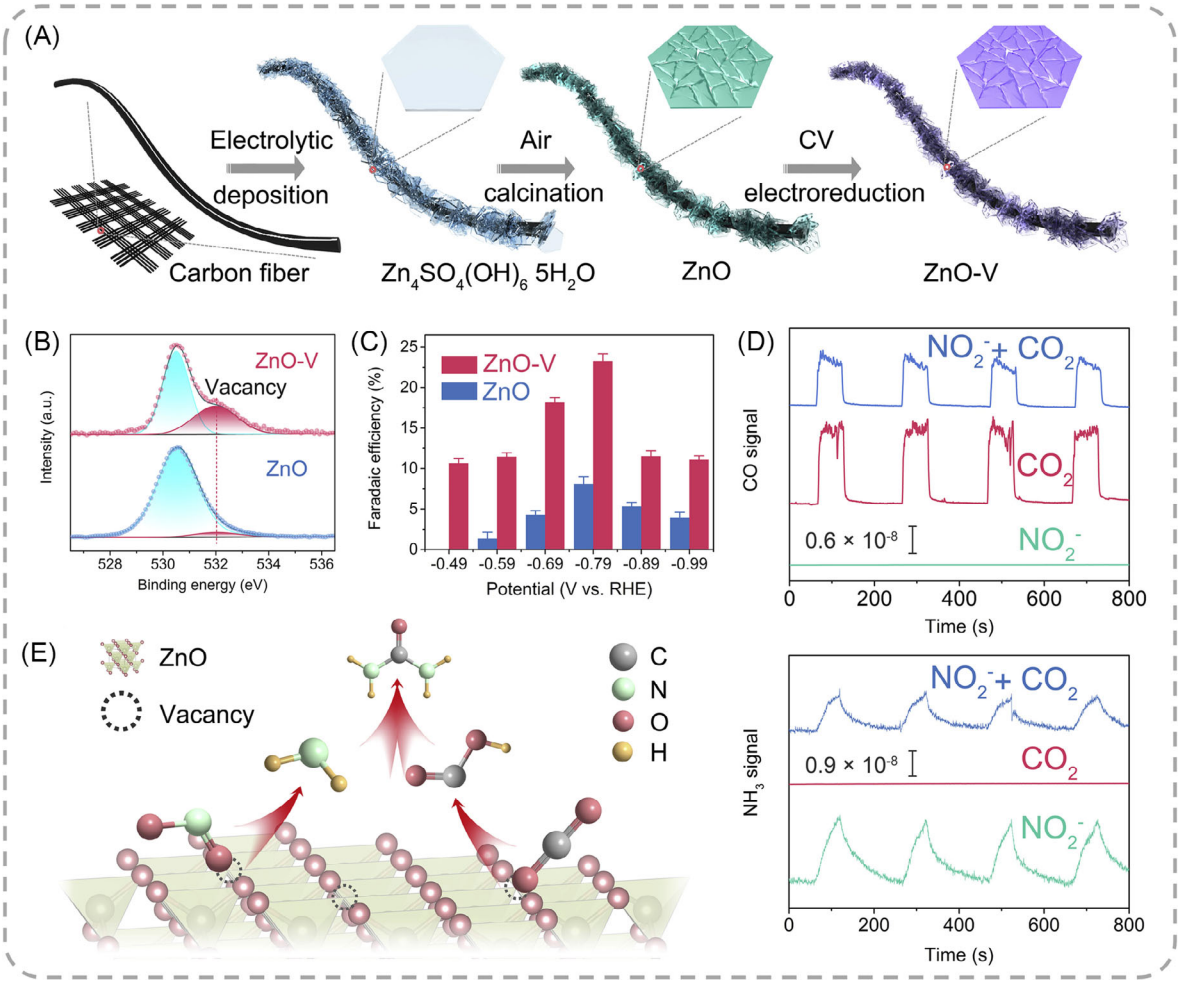

FIGURE 4 (A) Schematic representation of the synthesis of porous ZnO–V nanosheets. (B) O 1s X-ray photoelectron spectroscopy (XPS) and (C) Faradaic efficiency (FE) of urea under different potentials for ZnO and ZnO–V porous nanosheets. (D) Online differential electrochemical mass spectrometry (DEMS) spectra from CO and NH_3 signals arising from ZnO–V catalyst. (E) Illustration of urea electrosynthesis over ZnO–V.[81]

Moreover, to promote the electrosynthesis of urea via the coreduction of CO_2 and NO_2^- at a large scale, the development of an efficient electrode is essential. A monolithic electrode, with the advantages of having numerous active sites, reasonable electrical conductivity, and no need for a binder has been widely used in the electrocatalytic field.[80] Zhang and coworkers prepared self-supported OV-abundant ZnO (ZnO-V) porous nanosheets as a monolithic electrode for urea production.[81] The electrode preparation took place by a three-step method (Figure 4A). Firstly, carbon cloth was utilized to grow the nanosheet precursor by electrodeposition. Subsequently, the precursor was calcined in air to form porous ZnO nanosheets, leading to the generation of a porous structure by the release of gas from the precursor decomposition. In the end, ZnO was transformed to ZnO–V by electrochemical cyclic voltammetry reduction. The O 1s X-ray photoelectron spectroscopy (XPS) spectrum indicates that ZnO–V exhibits plentiful OVs (Figure 4B). When applied to the electrocatalytic coreduction of CO_2 and NO_2^-, ZnO–V shows an FE of 23.26% and a production rate of 16.56 μmol h^{-1}, which is much higher than the value of ZnO (Figure 4C). The online differential electrochemical mass spectrometry (MS) results show CO and NH_3 reduction with the coreduction of CO_2 and NO_2^- (Figure 4D), confirming the competitive reduction between CO_2 and NO_2^- on OVs. Combined with various characterizations and analysis results, one possible reaction pathway can be deduced as follows (Figure 4E): first, an oxygen atom in NO_2^- is inserted into one surface OV, followed by multistep proton-coupled electron transfer processes to NH_2*. Then, an oxygen in CO_2 is inserted into another surface OV to form COOH* intermediate after proton-coupled electron transfer. In the end, the NH_2* and COOH* intermediates couple via C–N bonds to synthesize urea. Undoubtedly, this OV modulation strategy in monolithic electrodes can offer valuable insights aiming to

construct more efficient vacancy-rich electrocatalysts for the coreduction of CO_2 and NO_2^-.

2.3 | NO_3^- as the nitrogenous species

Currently, there is global attention concerning the presence of NO_3^- in groundwater due to the large use of fertilizers and other anthropogenic sources, such as the discharge of domestic and industrial wastewater. As groundwater is one of the main sources of drinking water, numerous plants worldwide are focused on treating NO_3^- pollutants from it.[82] Among these methods, the electrocatalytic reduction of NO_3^- is an attractive option due to its eco-friendly nature. When coupled with CO_2 coreduction, urea can be synthesized via the C–N coupling process.[83] Nevertheless, large amounts of intermediates from NO_3^- reduction[84] and CO_2 reduction[85] can be present, leading to the generation of various undesirable products, such as NO_2^-, NH_3, CO. The sophisticated design of electrocatalysts is of critical importance to improve the catalytic activity for urea formation. In this section, several kinds of typical electrocatalysts are summarized to elucidate the research progress (Table 2), shedding light on the direction of urea electrosynthesis from the simultaneous reduction of CO_2 and NO_3^-.

Cu-based electrocatalysts have been widely used and have proven to be predominant catalysts for electrocatalytic CO_2 reduction due to their suitable binding energies for reductive intermediates.[106–108] For example, Kwon and coworkers found that Cu with atomic-scale spacing (*d*s) between its facets can effectively improve the electrocatalytic activity for urea synthesis (Figure 5A).[86] Cu_2O samples, with a series of interparticle *d*s values ranging from 3 to 15 Å, were prepared by controlling the lithiation degree. Among them, Cu with *d*s close to 6 Å can achieve an extremely high urea yield of 7541.9 μg h^{-1} mg_{cat}^{-1} and an FE_{urea} of 51.97%, in a gas-tight flow-type cell (Figure 5B). The partial current density of urea is 18.8-fold larger than the value of pristine Cu, which can achieve 115.25 mA cm^{-2}. The in situ X-ray absorption near edge structure and in situ Raman experiments, combined with the specific and electrochemical surface area tests and analyses, indicate that the catalytic performances are not originating from the modulation of oxidation state or surface area, but are affected by the atomic-scale distance between two facets over Cu nanoparticles. Density functional theory (DFT) modulations reveal that Cu with 6.0 Å *d*s can significantly lower the energy barrier for the critical C–N coupling, stemming from the top copper surface stabilizing the transition states of the reaction.

In addition to the geometric structure modulation over Cu-based monometallic electrocatalysts for the simultaneous electrocatalytic reduction of CO_2 and NO_3^-, the electronic structure can also be modulated to enhance the catalytic performance for Cu-based monometallic electrocatalysts. This modulation can help to promote the electrocatalytic simultaneous reduction of CO_2 and NO_3^- through C–N coupling. For example, Wang and coworkers discovered that in situ formed Cu^0–Cu^+ sites can thermodynamically and kinetically promote the asymmetric coupling process between *CO and *NO.[87] They first synthesized solid (s-Cu_2O), multihole (m-Cu_2O), and fragment (f-Cu_2O) Cu_2O nanospheres through chemical reduction combined with diluted hydrochloric acid etching. In situ Raman experiments indicate that the multihole Cu_2O could maintain the Cu^+ species under reaction conditions to form paired Cu^0–Cu^+ sites (Figure 5C,D). The Cu^0–Cu^+ sites promote the asymmetric coupling between *NO and *CO intermediates to form *ONCO. This design is able to achieve an impressive urea yield rate of 29.2 mmol h^{-1} g^{-1}, which is higher than that of s-Cu_2O and f-Cu_2O with the reconstructed Cu^0-dominant surface (Figure 5E).

Moreover, the Cu coordination structure also plays a crucial role in the electrocatalytic performance for the simultaneous reduction of CO_2 and NO_3^- to produce urea.[88] By modulating the temperature from 800°C to 1000°C in the pyrolysis step, during the catalyst preparation process, the prepared Cu single-atom catalysts show a change from Cu–N_4 coordination to Cu–N_{4-x}–C_x coordination (Figure 5F). The Cu–N_4 sites exhibit better activity for CO_2 reduction, while the Cu–N_4 and Cu–N_{4-x}–C_x sites are all effective in NO_3^- reduction. Theoretical analyses reveal that the generation of the *COOH intermediate is the rate-determining step for both CO_2RR and urea production. Therefore, the Cu–N_4 sites are more favorable for urea electrosynthesis (Figure 5G,H). The Cu-GS-800 catalyst can achieve an FE of 28% and a yield rate of 1840 μg h^{-1} mg^{-1}.

Cu-based bimetallic electrocatalysts have been rational designed for CO_2 and NO_3^- coreduction to further improve the activity for urea synthesis. In these catalysts, two kinds of metals serve as paired sites for adsorbing and activating CO_2 and NO_3^-, respectively.[89–91] Previous research has demonstrated that: (1) the C–N coupling process between *CO and *NH_2 species is the rate-determining step for urea synthesis[92]; (2) the reaction kinetics of C–N coupling process relies on the adsorption strength of *NH_2 and *CO, and their corresponding surface coverages, with high surface coverage enhancing the C–N coupling rate; and (3) the *CO intermediate from CO_2 reduction can accelerate the hydrodeoxidation of *NO_x intermediates to form *NH_2.[109] Based on these results, Wu and coworkers designed a Cu/ZnO stacked cascade gas-diffusion electrode (GDE), in which the ZnO catalyst layer

TABLE 2 Summary of urea electrosynthesis from CO_2 and NO_3^-.

Catalyst	Electrolyte	Cell type	Potential (V vs. RHE)	FE (%)	Partial CD (mA cm^{-2})	Yield	Ref.
6 Å-Cu	1 M KOH 0.1 M KNO_3	Flow cell	−0.41	51.97	115.25	7541.9 μg h^{-1} mg^{-1}	86
Multihole Cu_2O	0.1 M $KHCO_3$ 0.01 M KNO_3	H cell	−1.3	9.43	1.97	29.2 mmol h^{-1} g^{-1}	87
Cu-GS-800	0.1 M $KHCO_3$ 0.1 M KNO_3	H cell	−0.9	28	7.56	1840 μg h^{-1} mg^{-1}	88
Cu/ZnO	0.1 M KNO_3	Flow cell	−0.3	37.4	~1.12	12.8 mmol h^{-1} g^{-1}	89
$CuWO_4$	0.1 M KNO_3	H cell	−0.2	70.1	0.95	98.5 μg h^{-1} mg^{-1}	90
Pd–Cu/CBC	0.05 M KNO_3	H cell	−0.4	69.1	~1.38	763.8 μg h^{-1} mg^{-1}	91
Cu@Zn nanowires	0.2 M $KHCO_3$ 0.1 M KNO_3	H cell	−1.02	9.28	3.13	7.29 μmol cm^{-2} h^{-1}	92
Ru–Cu CF	0.1 M $NaNO_3$	Single cell	−0.13	25.4	~2.54	151.6 μg h^{-1} cm^{-2}	93
RhCu nanospheres	0.1 M KNO_3	H cell	−0.6	34.82	~0.17	26.81 mmol h^{-1} g^{-1}	94
$Cu_{97}In_3$–C	0.1 M $KHCO_3$ 0.01 M KNO_3	H cell	−1.4	~5	~1.25	13.1 mmol h^{-1} g^{-1}	95
Cu_1–CeO_2	0.1 M $KHCO_3$ 0.05 M KNO_3	H cell	−1.6	~5.5	~4.68	52.84 mmol h^{-1} g^{-1}	42
3D Zn/Cu	0.1 M $KHCO_3$ 1000 ppm KNO_3	Flow cell	−0.8	63	~10.00	59.5 mmol h^{-1} g^{-1}	96
MoO_x/C	0.1 M KNO_3	H cell	−0.6	27.7	~1.11	1431.5 μg h^{-1} mg^{-1}	97
Fe(a)@C–Fe_3O_4/CNTs	0.1 M KNO_3	H cell	−0.65	16.5	~0.50	1341.3 μg h^{-1} mg^{-1}	98
$In(OH)_3$–S	0.1 M KNO_3	H cell	−0.6	53.4	~0.53	533.1 μg h^{-1} mg^{-1}	41
Vo-InOOH	0.1 M KNO_3	H cell	−0.5	51.0	~0.36	592.5 μg h^{-1} mg^{-1}	99
Vo-CeO_2-750	0.1 M $KHCO_3$ 0.05 M KNO_3	H cell	−1.6	~3.8	~1.52	943.6 mg g^{-1} h^{-1}	100
Diatomic Fe–Ni	0.1 M $KHCO_3$ 0.05 M KNO_3	H cell	−1.5	17.8	~7.57	20.2 mmol h^{-1} g^{-1}	101
CoPc-COF@TiO_2	0.3 M $KHCO_3$ 0.2 M KNO_3	Flow cell	−0.6	49	~7.35	1205 μg h^{-1} cm^{-2}	102
F-CNT-300	0.1 M KNO_3	H cell	−0.65	18.0	0.30	6.36 mmol h^{-1} g^{-1}	103
Co_1–TiO_2	0.9 M $KHCO_3$ 0.1 M KNO_3	H cell	−0.80	36.2	18.4	212.8 mmol h^{-1} g^{-1}	104
NC	0.1 M $KHCO_3$ 0.1 M KNO_3	H cell	−0.5	62	~0.55	596.1 μg mg^{-1} h^{-1}	105

Abbreviations: CBC, carbonized bacterial cellulose; CD, current density; CF, copper foam; CNT, carbon nanotubes; FE, Faradaic efficiency; GS, graphene sheets; NC, nitrogen-doped carbon; Pc-COF, phtalocyanine-based covalent organic framework; RHE, reversible hydrogen electrode.

at the upstream helps to provide a concentrated CO to the following Cu catalyst layer (Figure 6A).[89] The high CO concentration leads to a high *CO surface coverage, promoting the NO_3^- conversion to *NH_2 on the Cu surface, resulting in a high *NH_2 surface coverage (Figure 6B). Consequently, the C–N coupling step is enhanced for urea electrosynthesis, leading to an FE of 37.4% with an urea yield rate of 12.8 mmol h^{-1} g_{cat}^{-1} (Figure 6C).

In addition, inspired by the efficient nitrate reduction facilitated through the natural Mo-based active center with high valence in nitrate reductase, Li and coworkers designed a $CuWO_4$ catalyst with a high-valence W active center. Bimetallic W and Cu with alternating sites can achieve a low formation overpotential and suitable adsorption ability for *NO_2 and *CO (Figure 6D).[90] As a result, the prepared $CuWO_4$ achieved an FE of 70.1 ± 2.4% and a high yield of 98.5 ± 3.2 μg h^{-1} mg_{cat}^{-1} (Figure 6E). A mechanistic study revealed that the direct coupling between *NO_2 and *CO has a lower energy barrier, resulting in favorable C–N coupling for urea generation (Figure 6F). Recently, it has been reported that when wastewater-level nitrate concentrations of 1000 ppm NO_3^- are used as a nitrogen source, a three-dimensional Zn/Cu heterostructure catalyst can lead to an urea yield rate of 59.5 mmol h^{-1}

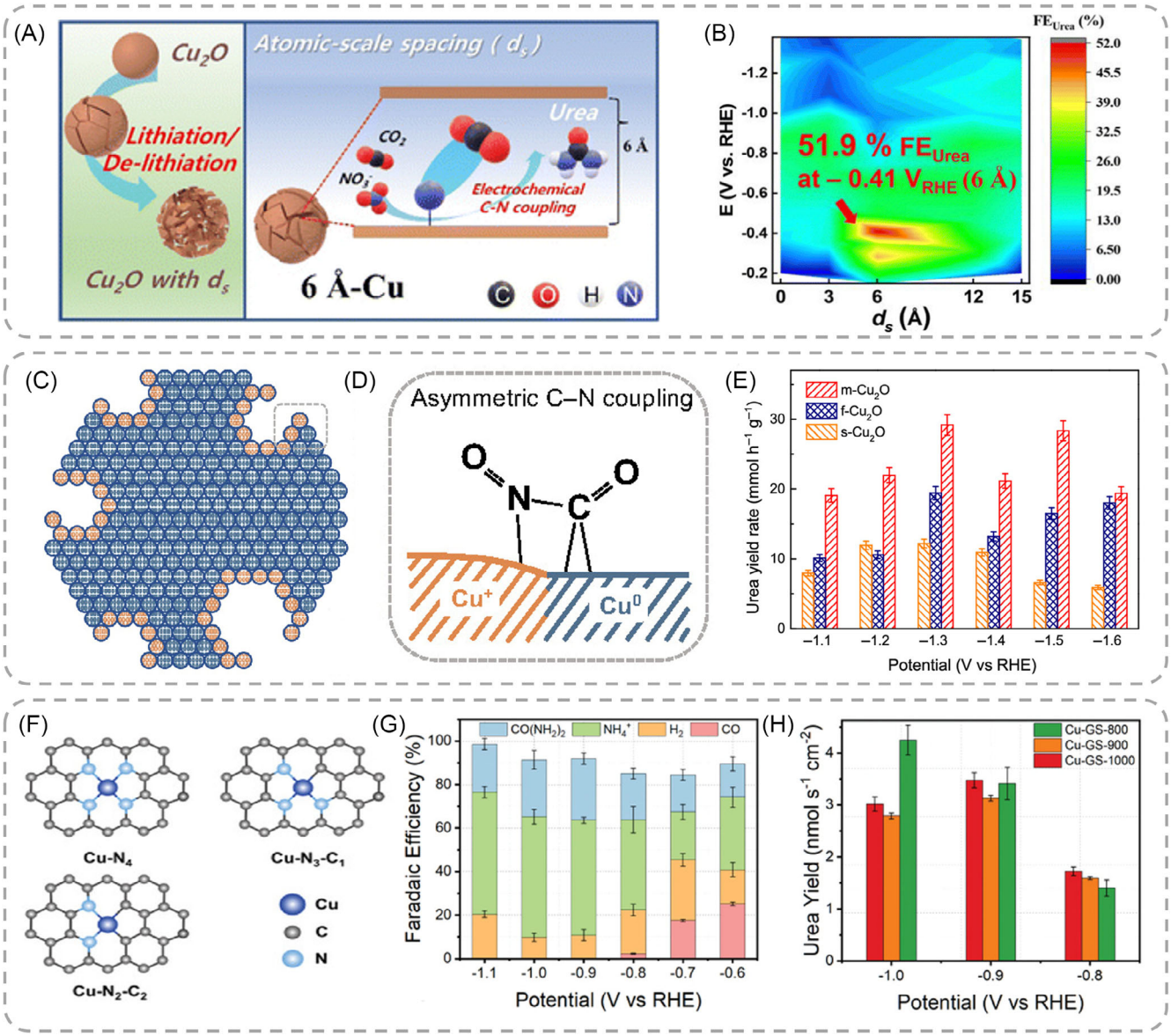

FIGURE 5 Cu-based monometallic electrocatalysts for urea synthesis from CO_2 and NO_3^-. (A) Schematic illustration of Cu with *ds* for urea synthesis. (B) Contour plot for the comparison of urea selectivity in terms of *ds* and reduction potentials.[86] (C) Multihole Cu_2O sphere preserving the Cu^+ component. (D) A formed Cu^0–Cu^+ site promoting C–N coupling step. (E) Electrocatalytic activity for urea synthesis.[87] (F) The atomic structures of Cu single-atom catalysts. (G) Selectivity for Cu-GS-800. (H) Electrocatalytic activity for urea synthesis over a series of Cu single-atom catalysts.[88]

g_{cat}^{-1}, with a catalyst loading of 0.27 mg cm^{-2} in the flow cell.[96]

Above all, despite the C–N coupling process originating from various N-containing and the C-containing intermediates used for C–N coupling over different catalysts, the Cu-based bimetallic strategy is able to provide two kinds of active sites for the corresponding intermediates. This offers a promising direction for developing efficient catalysts for urea electrosynthesis.

In addition to Cu-based electrocatalysts for the coreduction of CO_2 and NO_3^-, other metal-based electrocatalysts have also been developed to produce urea. For example, Qin and coworkers synthesized MoO_x nanoclusters supported on carbon black (Mo_xO/C) via a simple sonochemical deposition, dispersing around 1.4 nm MoO_x nanoclusters onto carbon black.[97] EXAFS spectra illustrate the coordination environment of Mo–O/C and Mo–Mo bonds over MoO_x/C catalyst (Figure 7A), with the EXAFS analysis indicating a lower coordination environment of 3.8 for the Mo atom. XPS results reveal a strong electronic interaction between MoO_x and carbon black via Mo–C heterointerfaces, facilitating electron transfer from carbon to MoO_x. Consequently, the highly unsaturated Mo sites with rich electrons prove beneficial for promoting

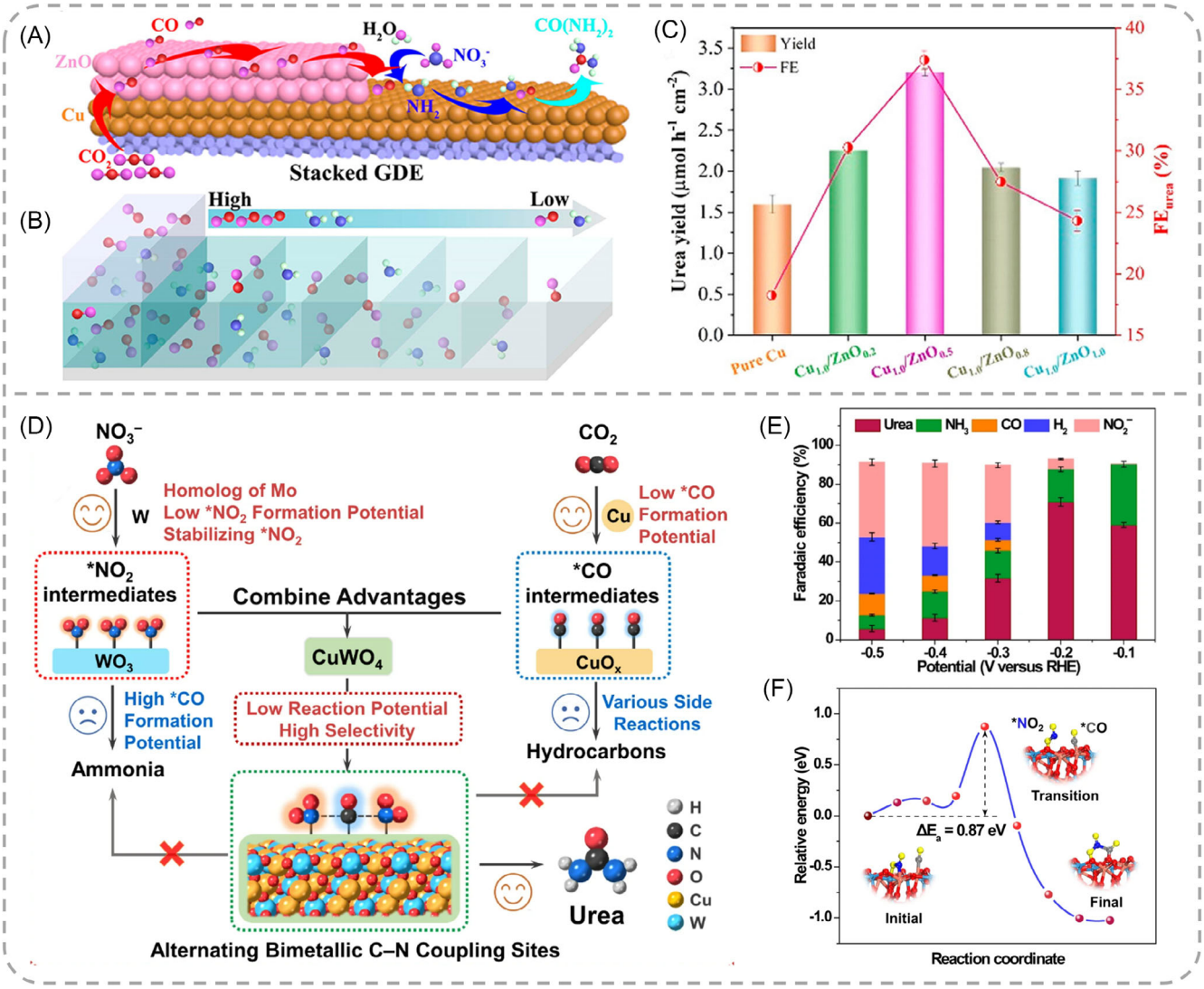

FIGURE 6 Cu-based bimetallic electrocatalysts for simultaneous reduction of CO_2 and NO_3^- to urea. (A) Schematic representation of Cu/ZnO tandem GDE. (B) Distribution of *CO and *NH_2 intermediate concentrations along the length of Cu GDE. (C) Electrocatalytic activity of stacked Cu/ZnO GDE.[89] (D) Schematic illustration of bioinspired alternating bimetallic sites of the $CuWO_4$ catalyst. (E) Electrocatalytic activity of $CuWO_4$. (F) Reaction mechanism of the C–N coupling process.[90]

the multielectron-involved reaction pathway in urea production. The catalyst achieves the highest FE of 27.7%, with an urea yield rate reaching 1431.5 μg h^{-1} mg$_{cat}^{-1}$, demonstrating excellent stability (Figure 7B). DFT calculations show that *NO_2 is more favorable for coupling with CO_2 to *CO_2NO_2 intermediate, and the hydrogenation step of *CO_2NO_2 to *CO_2NOOH is kinetically favorable on MoO_x/C (Figure 7C,D). Thus, the electron-abundant and unsaturated MoO_x clusters can help to alter the rate-determining route, and lower the required reaction energy barrier.

Moreover, Fe-based catalysts, extensively explored for electrocatalytic ammonia synthesis[110,111] and CO_2 reduction,[112,113] are a promising alternative for C–N coupling to urea. Zhang and coworkers obtained symbiotic iron oxide nanoparticles and graphitic carbon-encapsulated amorphous iron onto carbon nanotubes (Fe(a)@C–Fe_3O_4/CNTs), achieving an urea yield of 1341.3 μg h^{-1} mg^{-1} with an FE of 16.5% for the simultaneous reduction of CO_2 and NO_3^-.[98] Additionally, In-based catalysts,[41,99] OV-enriched CeO_2,[100] noble metals,[114] and some atomically dispersed catalysts[101,102,115] have already been used to produce urea. Recently, carbon-based metal-free materials have also been synthesized for urea synthesis.[103] This research progress provides a significant reference for developing highly efficient electrocatalysts for urea electrosynthesis from simultaneous reduction of CO_2 and NO_3^-.

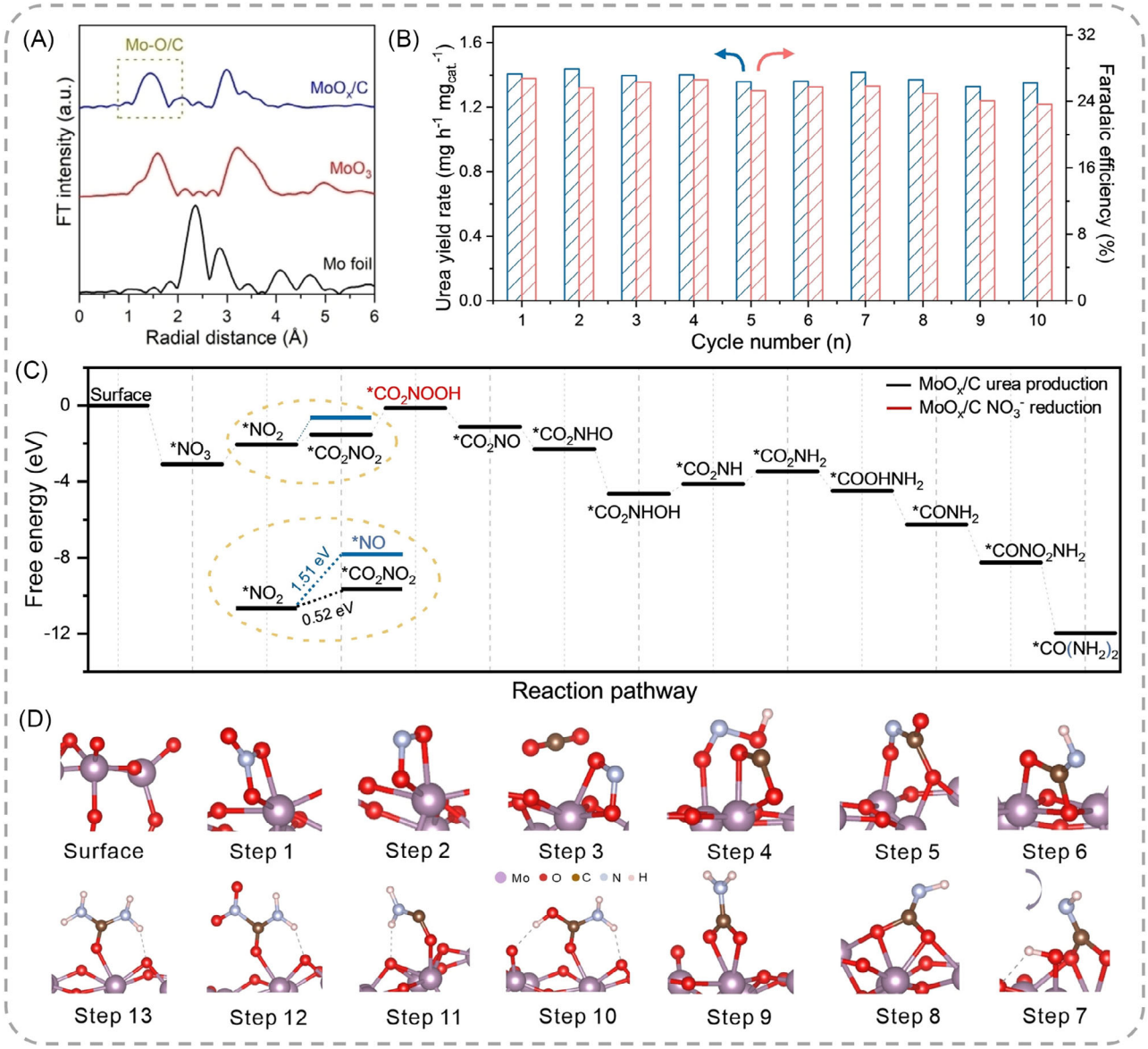

FIGURE 7 Molybdenum oxide nanoclusters for urea electrosynthesis. (A) Extended X-ray absorption fine structure (EXAFS) spectra of MoO_x/C. (B) Electrocatalytic stability test over 10 cycles under the reaction potential. (C) Diagram of Gibbs free energy change for producing urea using MoO_x/C catalyst and (D) the corresponding atomic configurations for each step.[97]

3 | ELECTROCATALYTIC C–N COUPLING TO AMIDE

Amides have a broad range of practical applications, including in polymers, pesticides, and pharmaceuticals.[116,117] They can be synthesized from CO_2 and nitrogenous species. Li and Kornienko developed a novel electrosynthetic pathway, in which NH_3 from the liquid electrolyte reacts with gaseous CO_2 over a solid Cu catalyst, which proceeds at a gas–liquid–solid three phase interface.[118] Formamide and acetamide were first synthesized from CO_2 and NH_3 through several proton coupling electron transfer steps. Optimization of Cu loading, KOH concentration and cation identity was performed to enhance amide generation. A higher Cu loading amount (10 vs. 2 mg cm^{-2}) showed the most significant enhancement in acetamide generation, attributed to the larger amount of highly reduced C_2 intermediates via a thicker Cu layer (Figure 8A,B). A relatively lower KOH concentration and a shift from potassium to caesium for electrolyte could also enhance the acetamide selectivity, possibly due to a more feasible local reaction environment that stabilized C_2 species, followed by coupling with NH_3. These optimizations were not suitable for enhancing formamide generation, which depends more on the C_1 intermediate coupling with NH_3. Using these optimized

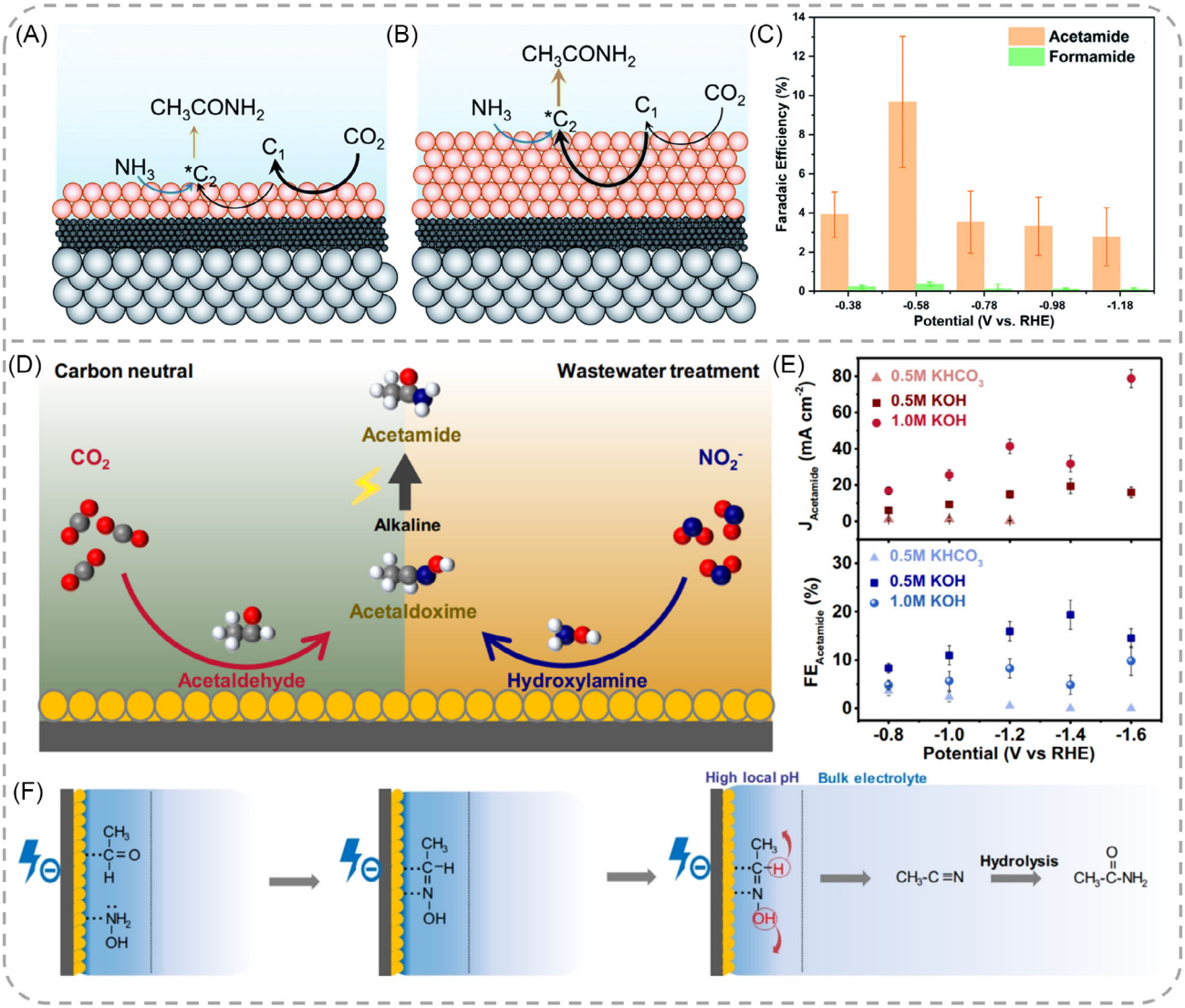

FIGURE 8 Electrocatalytic amide generation from carbonaceous and nitrogenous species. (A) Thin layers of Cu loading favor the formation of C_1 products, while (B) thicker layers further reduce C–N bond formation. (C) Electrocatalytic performance for amide generation at the optimized Cu loading.[118] (D) Illustration of acetamide production from CO_2 and nitrite. Electrocatalytic performance (E), and the schematic of reaction process and corresponding intermediates (F) for acetamide formation.[119]

parameters (0.1 M CsOH electrolyte and 10 mg cm^{-1} catalytic loading), an FE of approximately 10% for acetamide can be achieved (Figure 8C). This work is significant as it unveiled the first synthesis of formamide and acetamide from CO_2 and NH_3 building blocks, providing in-depth insights for understanding the reaction and improving the efficiency of these C–N coupling process.

To further increase the catalytic activity and extend the categories of nitrogen sources for amide generation, Ma and coworkers utilized CO_2 and NO_2^- as the raw materials to synthesize acetamide (Figure 8D).[119] In traditional H-type cell, the coreduction of CO_2 and NO_2^- are performed in neutral condition. Using this method, the formed acetaldehyde intermediate can be directly reduced to ethylamine.[120] Therefore, the flow cell with gas diffusion electrode is a preferred choice that can optimize the local reaction environment, and more importantly, the reduction current density can be enhanced by overcoming the limitation of CO_2 solubility. Based on these factors, the authors developed Cu nanoparticles, as the cathodic catalyst, deposited onto the gas diffusion layer in flow cell. When the coreduction of CO_2 and NO_2^- was performed in 0.5 M KOH, acetamide was produced within a broad range of applied potential, achieving the highest FE of 20% with approximately 20 mA cm^{-2} over the partial current density (Figure 8E). However, when 0.5 M $KHCO_3$ was chosen as the catholyte, the major C–N coupling products was switched to ethylamine with only about 2% FE for acetamide. The partial current density can be further enhanced to reach 80 mA cm^{-2} via using 1.0 M KOH

as cathodic electrolyte. In situ electrochemical attenuated total reflection Fourier transformed infrared spectroscopy characterization combined with DFT calculations indicate that acetaldehyde and hydroxylamine are the corresponding reaction intermediates resulting from the CO_2 and NO_2^- reduction, after that, a nucleophilic attack reaction takes place to form acetaldoxime. Next, the local alkaline reaction environment and electric field promote the dehydration process over acetaldoxime to acetonitrile, then the hydrolysis to acetamide (Figure 8F). This example gives a critical reaction paradigm and enlightening mechanism insight for amide generation from coreduction of CO_2 and nitrogenous species.

When alkaline electrolytes are employed for CO_2 reduction, the inevitable formation of undesired carbonates/bicarbonates leads to a lower CO_2 utilization rate and susceptibility to mass transfer issues in flow cells or MEA cells.[121–123] These challenges can be mitigated through a two-step CO_2 reduction. Initially, CO_2 is electrochemically reduced to CO under nonalkaline conditions, followed by the reduction of CO to the desired products.[124,125] Jiao and coworkers addressed these issues by synthesizing acetamide with almost 40% FE at a current density of 300 mA cm^{-2} via coelectrolysis of CO and NH_3 in a flow cell. In this setup, Cu cathodes are made through coating commercial Cu nanoparticles onto the gas-diffusion layer (GDL), and CO and NH_3 are co-fed into the gas channel.[126] Mechanism studies indicate that a ketene reaction intermediate is generated on Cu surface. This ketene intermediate is then nucleophilically attacked by NH_3 to form acetamide. Since ketene can also react with other nucleophilic agents with amine groups, additional amines, such as methylamine, ethylamine, and dimethylamine, have been introduced during CO electrolysis. Consequently, N-methylacetamide, N-ethylacetamide, and N,N-dimethylacetamide achieved FEs of 42%, 34%, and 36%, respectively, at 300 mA cm^{-2}. This strategy, involving a nucleophilic attack on a ketene intermediate during CO_2/CO electroreduction, opens avenues to produce a wide range of valuable chemicals containing C–N bonds in future research.

In addition to the coupling of CO with nitrogenous species for amide synthesis, formic acid from electrocatalytic CO_2 reduction serves as an efficient carbon source for amide production.[127–129] For instance, Zhang and coworkers demonstrated the synthesis of formamide from formate and nitrite, with Cu displaying superior catalytic activity compared to other metallic catalysts.[130] Utilizing an electrochemical reduction method, low-coordinated Cu (denoted as ER-Cu), with large amounts of active sites and appropriate binding energy with intermediates, was synthesized from Cu_2O nanocubes. EXAFS results reveal a much lower Cu–Cu peak intensity in ER-Cu compared to Cu foil, which confirms the successful formation of low-coordinated Cu. When applied in electrocatalytic formamide production in 0.5 M NaOH with 0.2 M HCOOH and 0.02 M $NaNO_2$, FE reaches up to 29.7% at −0.4 V versus RHE, with a yield of 35.1 mmol h^{-1} g_{cat}^{-1} at −0.6 V versus RHE. Control experiments with various C and N sources reveal that formamide originates from formate and nitrite, and the latter can be replaced with nitrate for formamide generation. Additionally, acetamide can also be synthesized when ethanoic acid is chosen as the C source. Electrochemical in situ characterizations, combined with DFT modulations, allow to elucidate the synthetic progress of C–N bonds by coupling *CHO with *NH_2 intermediates, which spontaneously occurs on the low-coordinated Cu surface. Consequently, formamide can be efficiently synthesized using CO_2-derived formic acid and nitrite/nitrate contaminants.

4 | ELECTROCATALYTIC C–N COUPLING TO AMINE

Methylamine, the simplest alkylamine, is a crucial raw material for fine chemicals, including pesticides and pharmaceuticals. These compounds are typically manufactured through the gas-phase reaction of ammonia and methanol in industrial processes, carried out under high temperature and pressure.[131] In contrast, the electrocatalytic reduction of CO_2 and NO_3^- to methylamine can occur in aqueous media under mild conditions. Wang and coworkers pioneered the electrocatalytic synthesis of methylamine from CO_2 and NO_3^-, using cobalt β-tetraaminophthalocyanine supported on CNTs (Figure 9A).[132] Methylamine can achieve an optimal FE of 13% with a partial current density reaching 3.4 mA cm^{-2}. Importantly, the electrolysis remains stable during the stability test (Figure 9B). The mechanistic study reveals a detailed eight-step electrocatalytic cascade involving the transfer of 14 electrons and 15 protons in the synthesis of methylamine. HCHO and NH_2OH are initially produced from CO_2 and NO_3^- reduction. Subsequently, the adsorbed HCHO experiences a nucleophilic attack by NH_2OH to form formaldoxime, leading to the reduction to N-methylhydroxylamine and ultimately forming methylamine.

In addition, Xiao and coworkers achieved a deep understanding of the reaction mechanism of methylamine electrosynthesis through comprehensive studies of the C–N coupling process. DFT modulations and reaction phase diagram analysis have been employed to consider all possible pathways based on the provided reactants and products (Figure 9C).[133] Among these pathways, r_A, r_B, and r_C denote the largest reaction free energies identified through

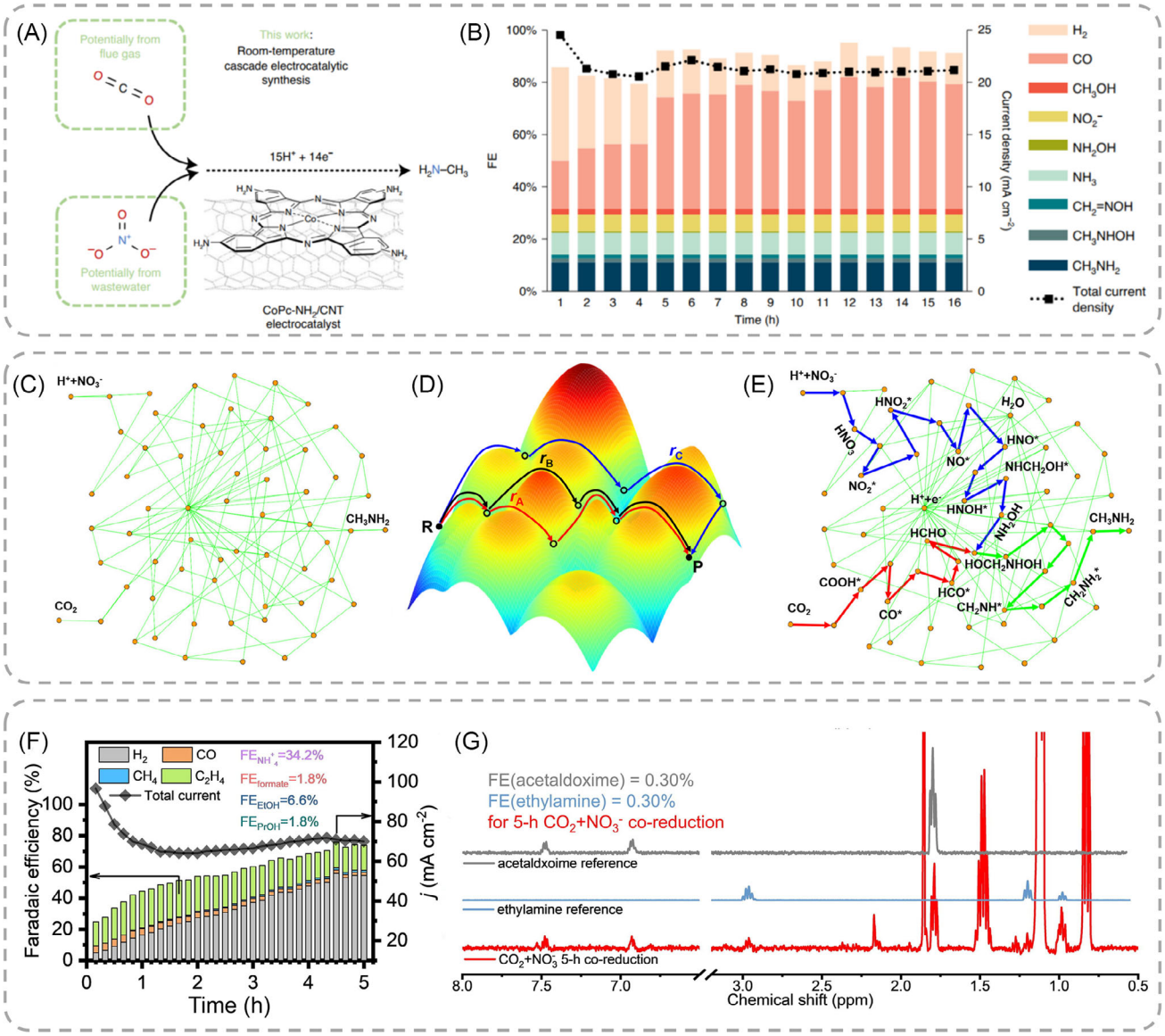

FIGURE 9 Amine generation from the reduction of carbonaceous and nitrogenous species. (A) Illustration of methylamine electrosynthesis from CO_2 and NO_3^-. (B) Product distribution and total current density during the stability test.[132] (C) Complex reaction network for methylamine generation from CO_2 and NO_3^-. (D) Optimal reaction pathway via global energy optimization, where the redder color indicates higher energy. (E) Specific pathways for methylamine formation.[133] (F) Product distribution and total current density for simultaneous reduction of CO_2 and NO_3^-. (G) ^{1}H nuclear magnetic resonance (NMR) spectrum of the electrolyte after reaction.[120]

internal comparisons. The red pathway, determined as the optimal pathway due to the smallest free energies (Figure 9D), was derived by the principle of global optimization energy (Figure 9E). Notably, the C–N coupling reaction between desorbed HCHO and NH_2OH is more feasible than both species being adsorbed onto the electrocatalyst. Kinetic barrier and microkinetic calculations permit a further elucidation on the FE trends of methylamine at different reaction potentials, providing in-depth insights for promoting methylamine activity and selectivity. These findings guide the sophisticated design of electrocatalysts to enhance methylamine production.

Ethylamine is another kind of vital alkylamine in chemical synthesis and pharmaceutical chemistry. Currently, there are several technologies for ethylamine synthesis in industry, however, they are typically operated in harsh conditions. For example, the amination of alcohols occurs at high temperature and high pressure with ethanol and ammonia as raw materials.[134,135] Recently, Wang and coworkers first reported the simultaneous electrocatalytic reduction of CO_2 and NO_3^- to ethylamine via a 20-electron coupling 21-proton reduction.[120] An oxide-derived Cu nanoparticle catalyst was used under environmental conditions in a near-neutral electrolyte. The C–N coupling

product is acetaldoxime with a 16-electron coupling 17-proton reduction process, without ethylamine generation. When electrolysis is extended to 5 h, the FE of H_2 gradually increases, possibly due to proton production arising from NH_4^+ near the cathode surface (Figure 9F). More interestingly, ethylamine can be detected by ^{1}H NMR with an FE of 0.30% (Figure 9G). To unveil the reaction mechanism, the authors carried out controlled experiments with several C or N sources. As a result, a possible reaction pathway could be deduced as follows: CO_2 and NO_3^- are separately reduced to acetaldehyde and NH_2OH, which then chemically couple to form acetaldoxime, following by reduction to ethylamine. Although the yield rate is still very low for immediate practical application, this catalytic cascade enlightens the direction for the synthesis of C_{2+} amines products from low-cost and abundant sources via renewable electricity.

5 | SUMMARY AND OUTLOOK

This review initially provides a comprehensive overview of electrocatalytic C–N coupling reaction to urea from CO_2 and several nitrogenous species, detailing N_2, NO_2^-, and NO_3^- as N sources. Subsequently, it summarizes recent research developments in amide electrosynthesis, specifically focusing on formamide and acetamide. The discussion then delves into the design of electrocatalysts and mechanistic studies on amine formation.

While substantial progress has been made in expanding the range of C–N coupling products through electrocatalytic synthesis from CO_2 and nitrogenous species, there is still potential for synthesizing other kinds of C–N coupling chemicals.[136] Amino acids are valuable organic compounds with amino and carboxylic acid functional groups that are currently a focal point of recent research. Recently, Che and coworkers successfully obtained enantiomeric serine from CO_2 and NH_3, by utilizing chiral Cu films as electrocatalysts.[137] The research results highlight that the stereo-determining step for serine generation is the formation from H_2CO–CO* to 3-hydropyruvic acid. Chiral kink sites on chiral Cu films restrict the configuration of the stereoselective intermediates, favoring enantiomeric serine synthesis in both thermodynamical and kinetical aspects. Moreover, enzymatic electrosynthesis has successfully produced glycine from CO_2 and NH_3 through an in vitro multienzymatic cascade.[138] Optimizing individual modules in the enzymatic electrocatalytic system has resulted in the production of glycine (0.81 mM) with a remarkable FE of 96.8%. The electrocatalytic synthesis of C–N coupling compounds beyond urea is summarized in Table 3, highlighting diverse examples that illustrate the electrochemical synthesis of various organic compounds containing C–N bonds from CO_2 and nitrogen sources.

The production of C–N coupling products from CO_2 and nitrogenous species is theoretically carried out at the cathode. However, the slow anodic water oxidation requires a high applied potential, leading to lower energy efficiency.[141,142] If the anodic oxidation is replaced by the C–N coupling reaction with a lower applied potential, economic efficiency is significantly enhanced. Alcohols, serving as alternative carbon sources, can be initially produced from electrocatalytic CO_2 reduction. Notably, catalytic oxidation of alcohols allows the formation of aldehyde-like intermediates that can react with ammonia to generate amides.[143] During the electrooxidation of alcohols, the in situ formed formaldehyde-like intermediates are nucleophilically attacked by ammonia to form amides. Importantly, the liquid-phase C–N coupling reaction from alcohols and ammonia, with excellent solubility in water, would avoid mass-transport limitations, inevitably realizing a high yield rate.

Building on this concept, Zhang and coworkers have electrochemically synthesized formamide with methanol and ammonia over a Pt catalyst, resulting in 74.26% selectivity from methanol to formamide and an FE of 40.39% at 100 mA cm^{-2}.[144] Furthermore, a boron-doped diamond electrocatalyst has been employed for scalable synthesis of formamide. In this setup, an 8 L single-cell electrolyser possessing a 2200 cm^2 electrode area has been used, being powered by an external renewable power.[145] The formation of formamide achieves an FE of 33.5% at 120 mA cm^{-2} (total current: 264 A), exhibiting the large application prospects of this coupling strategy. More recently, the long-chain and aryl-ring amides have also been successfully synthesized from alcohols and amines with high selectivity.[146] This progress provides significant guidance for developing valuable C–N coupling products via anodic oxidation.

Understanding the C–N coupling mechanism is critical for guiding the sophisticated design of electrocatalysts and further improving the catalytic performance. However, the complex reaction microenvironment at the molecular or atomic level hinders the elucidation of the C–N coupling mechanism under real conditions. Although theoretical calculations have been rapidly developed to analyze the reaction process, the gap between the theoretical model and the true dynamic structure makes it challenging to fully uncover the real reaction mechanism. Therefore, the further development of in situ/operando analytic techniques would be significant in unveiling the evolution of catalysts and reaction intermediates during the reaction. Despite substantial progress in developing electrochemical in situ/operando methods, challenges persist in understanding the complex reaction process.[147,148] For example,

TABLE 3 Summary of C–N coupling compounds beyond urea.

Catalyst	Product	C/N resource	Cell type	Potential (V vs. RHE)	FE (%)	Partial CD (mA cm^{-2})	Yield	Ref.
ER-Cu	Formamide	HCOOH $NaNO_2$	H cell	−0.6	~25.0	~12.5	35.1 mmol h^{-1} g^{-1}	130
Ru_1Cu SAA	Formamide	CO KNO_2	H cell	−0.5	45.65	~5.5	2483.77 μg h^{-1} mg^{-1}	139
Cu NPs	Acetamide	CO NH_3	Flow cell	−0.68	38	114	–	126
Cu NPs	Acetamide	CO_2 NH_3	Flow cell	−0.58	10	~2.2	–	118
CoPc–NH_2/CNT	Methylamine	CO_2 KNO_3	H cell	−0.92	13	3.4	–	132
CuO NPs	Ethylamine	CO_2 KNO_3	H cell	−1.0	0.3	~0.21	–	120
Cu–Hg	Glycine	Oxalic acid $NaNO_3$	H cell	−1.4 V versus Ag/AgCl	43.1	–	–	140
Enzyme	Glycine	CO_2 NH_3	H cell	−1.2 V versus Ag/AgCl	96.8	–	8.69 mg L^{-1} h^{-1}	138
Chiral Cu films	Serine	CO_2 NH_3	H cell	CV	1.2	–	–	137

Abbreviations: CD, current density; FE, Faradaic efficiency; NPs, nanoparticles; RHE, reversible hydrogen electrode; SAA, single atom alloy.

some species detected by spectroscopic techniques are strongly anchored on the catalyst surface, functioning as mere spectators during the catalytic reaction. In some cases, the strongly anchored species could be detrimental to the electrocatalysts. Additionally, other key intermediates, present in small amounts, could play a dominant role in product generation, requiring the development of high-resolution characterization tools. On the other hand, the phenomenon of short-lived intermediates has not been adequately considered during in situ/operando analysis due to the time-resolved limitations of the current techniques, which operate on a time scale of seconds or minutes. Therefore, developing high time-resolved techniques in the time frame of milliseconds or picoseconds is of significant importance to capture the key intermediates during the reaction. Moreover, reaction kinetics should focus more on real C–N coupling mechanisms and establish structure–activity relationships over corresponding catalysts.[149]

In conclusion, the electrocatalytic synthesis of C–N coupling compounds from CO_2 and nitrogenous species presents an effective avenue for valuable chemicals generation and renewable energy storage. However, the current catalytic performance is still far from industrial application, primarily due to the low selectivity, activity, and stability. The key challenge in this field lies in the precise design of advanced catalysts to enhance C–N coupling performance. The classical strategies of modulating the electronic or geometric structures of electrocatalysts, such as adjusting oxidation state of metal catalysts, metal–support interaction, alloying, defect engineering, and single-atom or dual-atom catalysts, would be also suitable for C–N coupling reaction from CO_2 and nitrogen sources. However, these novel coupling reactions are generally performed through simultaneous coactivation of CO_2 and nitrogen sources, which requires catalysts with neighboring active sites. Accordingly, one active site is designed for CO_2 reduction to specific C-based intermediate, and the other is for generating N-based intermediates. Optimized catalysts are beneficial to promote the coupling reaction for these two intermediates, while C–C coupling and other side reactions can be effectively suppressed. Additionally, it is crucial to consider the economic cost associated with the preparation of electrocatalysts on a large scale.

Moreover, the design and optimization of electrochemical reactors for different C–N coupling reactions are essential aspects. While flow cells and MEA electrolysers find broad applications in electrochemically reducing CO_2, due to their ability to eliminate diffusion limitations and reduce energy consumption, the diffusion and mass transfer characteristics during the reaction vary for various feedstocks in the flow channel. This highlights the importance of a sophisticated design and operation of electrolysers, especially for specific C–N coupling reactions with industrial relevance. Although the research process from CO_2 reduction can provide references for C–N coupling reactions, the different reaction conditions need sophisticated optimization of each component

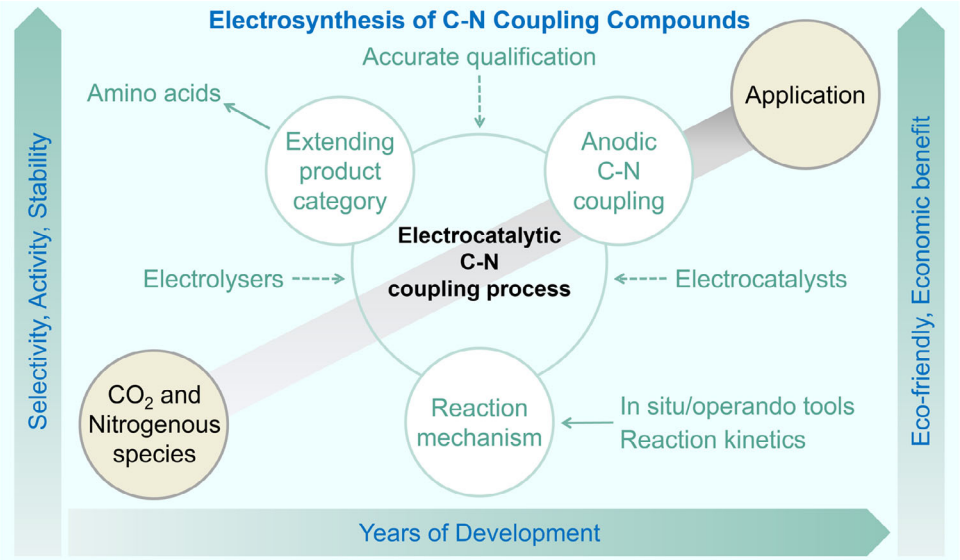

FIGURE 10 Challenges and perspectives for electrocatalytic synthesis of C–N coupling compounds.

in electrolysers. More importantly, rigorous detection of C–N coupling products requires increased attention to ensure reliable results.[150] Through these collective efforts (Figure 10), the electrosynthesis of C–N coupling compounds from CO_2 and nitrogenous species is likely to achieve practical applications in the near future.

ACKNOWLEDGMENTS

The authors gratefully acknowledge financial support from the National Natural Science Foundation of China (Nos. 42277485, 21976141, 22272197, 22102184, 22102136, and U22A20392), the Natural Science Foundation of Hubei Province (2022CFB1001 and 2021CFA034), the Department of Education of Hubei Province (Q20221701 and Q20221704), and the Joint Fund of Yulin University and Dalian National Laboratory for Clean Energy (YLU-DNL Fund 2022008). S.A.C.C. acknowledges FCT/MCTES, Fundação para a Ciência e Tecnologia and Ministério da Ciência, Tecnologia e Ensino Superior (projects DOIs: 10.54499/LA/P/0008/2020, 10.54499/UIDB/50006/2020 and 10.54499/UIDP/50006/2020) and the Scientific Employment Stimulus—Institutional Call (DOI: 10.54499/CEECINST/00102/2018/CP1567/CT0026).

CONFLICT OF INTEREST STATEMENT

The authors declare no conflict of interest.

ORCID

Zheng Zhang https://orcid.org/0000-0002-4800-1059
Sónia A. C. Carabineiro https://orcid.org/0000-0001-9913-4671
Xuping Sun https://orcid.org/0000-0001-5034-1135

REFERENCES

1. Service RF. Carbon capture marches toward practical use. *Science*. 2021;371(6536):1300.
2. Zhang Z, Zhao W, Nong J, et al. Liquid–solid phase-change behavior of diethylenetriamine in nonaqueous systems for carbon dioxide absorption. *Energy Technol*. 2017;5(3):461-468.
3. Sharifian R, Wagterveld RM, Digdaya IA, Xiang C, Vermaas DA. Electrochemical carbon dioxide capture to close the carbon cycle. *Energy Environ Sci*. 2021;14(2):781-814.
4. Hepburn C, Adlen E, Beddington J, et al. The technological and economic prospects for CO_2 utilization and removal. *Nature*. 2019;575(7781):87-97.
5. Zhao P, Jiang H, Shen H, et al. Construction of low-coordination Cu−C_2 single-atoms electrocatalyst facilitating the efficient electrochemical CO_2 reduction to methane. *Angew Chem Int Ed*. 2023;62(49):e202314121.
6. Zhang Z, Yu L, Tu Y, et al. Unveiling the active site of metal-free nitrogen-doped carbon for electrocatalytic carbon dioxide reduction. *Cell Rep Phys Sci*. 2020;1(8):100145.
7. Wang K, Zhu Y, Gu M, et al. A derivative of $ZnIn_2S_4$ nanosheet supported Pd boosts selective CO_2 hydrogenation. *Adv Funct Mater*. 2023;33(30):2215148.
8. Li Z, Qi X, Wang J, et al. Stabilizing highly active atomically dispersed NiN_4Cl sites by Cl-doping for CO_2 electroreduction. *SusMat*. 2023;3(4):498-509.
9. Liu G, Li X, Liu M, et al. Dimensional engineering of covalent organic frameworks derived carbons for electrocatalytic carbon dioxide reduction. *SusMat*. 2023;3(6):834-842.
10. Rochelle GT. Amine scrubbing for CO_2 capture. *Science*. 2009;325(5948):1652.
11. Nitopi S, Bertheussen E, Scott SB, et al. Progress and perspectives of electrochemical CO_2 reduction on copper in aqueous electrolyte. *Chem Rev*. 2019;119(12):7610-7672.
12. Wakerley D, Lamaison S, Wicks J, et al. Gas diffusion electrodes, reactor designs and key metrics of low-temperature CO_2 electrolysers. *Nat Energy*. 2022;7(2):130-143.

13. She X, Wang Y, Xu H, Tsang SCE, Lau SP. Challenges and opportunities in electrocatalytic CO_2 reduction to chemicals and fuels. *Angew Chem Int Ed*. 2022;61(49):e202211396.
14. Sang J, Wei P, Liu T, et al. A reconstructed $Cu_2P_2O_7$ catalyst for selective CO_2 electroreduction to multicarbon products. *Angew Chem Int Ed*. 2022;61(5):e202114238.
15. Li W, Yin Z, Gao Z, et al. Bifunctional ionomers for efficient co-electrolysis of CO_2 and pure water towards ethylene production at industrial-scale current densities. *Nat Energy*. 2022;7:835-843.
16. Zhang Z, Huang X, Chen Z, et al. Membrane electrode assembly for electrocatalytic CO_2 reduction: principle and application. *Angew Chem Int Ed*. 2023;62(28):e202302789.
17. Zhang G, Li L, Zhao ZJ, Wang T, Gong J. Electrochemical approaches to CO_2 conversion on copper-based catalysts. *Acc Mater Res*. 2023;4(3):212-222.
18. Li L, Li X, Sun Y, Xie Y. Rational design of electrocatalytic carbon dioxide reduction for a zero-carbon network. *Chem Soc Rev*. 2022;51(4):1234-1252.
19. Lv JJ, Yin R, Zhou L, et al. Microenvironment engineering for the electrocatalytic CO_2 reduction reaction. *Angew Chem Int Ed*. 2022;61(39):e202207252.
20. Tao Z, Rooney CL, Liang Y, Wang H. Accessing organonitrogen compounds via C–N coupling in electrocatalytic CO_2 reduction. *J Am Chem Soc*. 2021;143(47):19630-19642.
21. Li J, Zhang Y, Kuruvinashetti K, Kornienko N. Construction of C–N bonds from small-molecule precursors through heterogeneous electrocatalysis. *Nat Rev Chem*. 2022;6(5):303-319.
22. Zhang Y, Yu Q, Wang X, Guo W. Conversion of nitrogenous small molecules into value-added chemicals by building N–C bonds. *Chem Eng J*. 2023;474:145899.
23. Jiang H, Wu X, Zhang H, et al. Toward effective electrocatalytic C–N coupling for the synthesis of organic nitrogenous compounds using CO_2 and biomass as carbon sources. *SusMat*. 2023;3(6):781-820.
24. Peng X, Zeng L, Wang D, et al. Electrochemical C–N coupling of CO_2 and nitrogenous small molecules for the electrosynthesis of organonitrogen compounds. *Chem Soc Rev*. 2023;52(6):2193-2237.
25. Zhong Y, Xiong H, Low J, Long R, Xiong Y. Recent progress in electrochemical C–N coupling reactions. *eScience*. 2023;3(1):100086.
26. Liu S, Wang M, Cheng Q, et al. Turning waste into wealth: sustainable production of high-value-added chemicals from catalytic coupling of carbon dioxide and nitrogenous small molecules. *ACS Nano*. 2022;16(11):17911-17930.
27. Ye Y, Li Z, Ding S, Fu J, Liu H, Zhu W. Synergistic treatment of carbon dioxide and nitrogen-containing wastewater by electrochemical C–N coupling. *iScience*. 2023;26(7):107009.
28. Tang C, Qiao SZ. How to explore ambient electrocatalytic nitrogen reduction reliably and insightfully. *Chem Soc Rev*. 2019;48(12):3166-3180.
29. Qing G, Ghazfar R, Jackowski ST, et al. Recent advances and challenges of electrocatalytic N_2 reduction to ammonia. *Chem Rev*. 2020;120(12):5437-5516.
30. Liu Q, Xu T, Luo Y, et al. Recent advances in strategies for highly selective electrocatalytic N_2 reduction toward ambient NH_3 synthesis. *Curr Opin Electrochem*. 2021;29:100766.
31. Ouyang L, Liang J, Luo Y, et al. Recent advances in electrocatalytic ammonia synthesis. *Chin J Catal*. 2023;50:6-44.
32. Wan H, Wang X, Tan L, et al. Electrochemical synthesis of urea: co-reduction of nitric oxide and carbon monoxide. *ACS Catal*. 2023;13(3):1926-1933.
33. Xian J, Li S, Su H, et al. Electrocatalytic synthesis of essential amino acids from nitric oxide using atomically dispersed Fe on N-doped carbon. *Angew Chem Int Ed*. 2023;62(26):e202304007.
34. Zhang L, Liang J, Wang Y, et al. High-performance electrochemical NO reduction into NH_3 by MoS_2 nanosheet. *Angew Chem Int Ed*. 2021;60(48):25263-25268.
35. Liang J, Liu P, Li Q, et al. Amorphous boron carbide on titanium dioxide nanobelt arrays for high-efficiency electrocatalytic NO reduction to NH_3. *Angew Chem Int Ed*. 2022;61(18):e202202087.
36. Yue L, Song W, Zhang L, et al. Recent advance in heterogenous electrocatalysts for highly selective nitrite reduction to ammonia under ambient condition. *Small Struct*. 2023;4(11):2300168.
37. Liang J, Li Z, Zhang L, et al. Advances in ammonia electrosynthesis from ambient nitrate/nitrite reduction. *Chem*. 2023;9(7):1768-1827.
38. Song W, Yue L, Fan X, et al. Recent progress and strategies on the design of catalysts for electrochemical ammonia synthesis from nitrate reduction. *Inorg Chem Front*. 2023;10(12):3489-3514.
39. Cao N, Quan Y, Guan A, et al. Oxygen vacancies enhanced cooperative electrocatalytic reduction of carbon dioxide and nitrite ions to urea. *J Colloid Interface Sci*. 2020;577:109-114.
40. Liu S, Yin S, Wang Z, et al. AuCu nanofibers for electrosynthesis of urea from carbon dioxide and nitrite. *Cell Rep Phys Sci*. 2022;3(5):100869.
41. Lv C, Zhong L, Liu H, et al. Selective electrocatalytic synthesis of urea with nitrate and carbon dioxide. *Nat Sustain*. 2021;4(10):868-876.
42. Wei X, Liu Y, Zhu X, et al. Dynamic reconstitution between copper single atoms and clusters for electrocatalytic urea synthesis. *Adv Mater*. 2023;35(18):2300020.
43. Jiang M, Zhu M, Wang M, et al. Review on electrocatalytic coreduction of carbon dioxide and nitrogenous species for urea synthesis. *ACS Nano*. 2023;17(4):3209-3224.
44. Chen C, He N, Wang S. Electrocatalytic C–N coupling for urea synthesis. *Small Sci*. 2021;1(11):2100070.
45. Yu K, Wang H, Yu W, Li S, Zhang X, Bian Z. Resource utilization of carbon dioxide and nitrate to produce value-added organonitrogen compounds through an electrochemical approach. *Appl Catal B Environ*. 2024;341:123292.
46. Comer BM, Fuentes P, Dimkpa CO, et al. Prospects and challenges for solar fertilizers. *Joule*. 2019;3(7):1578-1605.
47. Rollinson AN, Jones J, Dupont V, Twigg MV. Urea as a hydrogen carrier: a perspective on its potential for safe, sustainable and long-term energy supply. *Energy Environ Sci*. 2011;4(4):1216-1224.
48. Zheng X, Yang J, Li P, et al. Dual-atom support boosts nickel-catalyzed urea electrooxidation. *Angew Chem Int Ed*. 2023;62(22):e202217449.
49. Schlögl R. Catalytic synthesis of ammonia—a "never-ending story"? *Angew Chem Int Ed*. 2003;42(18):2004-2008.
50. Soloveichik G. Electrochemical synthesis of ammonia as a potential alternative to the Haber–Bosch process. *Nat Catal*. 2019;2(5):377-380.

51. Giddey S, Badwal SPS, Kulkarni A. Review of electrochemical ammonia production technologies and materials. *Int J Hydrogen Energy*. 2013;38(34):14576-14594.
52. Kyriakou V, Garagounis I, Vourros A, Vasileiou E, Stoukides M. An electrochemical Haber–Bosch process. *Joule*. 2020;4(1):142-158.
53. Liu H. Ammonia synthesis catalyst 100 years: practice, enlightenment and challenge. *Chin J Catal*. 2014;35(10):1619-1640.
54. Wang Y, Chen D, Chen C, Wang S. Electrocatalytic urea synthesis via C–N coupling from CO_2 and nitrogenous species. *Acc Chem Res*. 2024;57(2):247-256.
55. Chen C, Zhu X, Wen X, et al. Coupling N_2 and CO_2 in H_2O to synthesize urea under ambient conditions. *Nat Chem*. 2020;12(8):717-724.
56. Yuan M, Chen J, Bai Y, et al. Electrochemical C–N coupling with perovskite hybrids toward efficient urea synthesis. *Chem Sci*. 2021;12(17):6048-6058.
57. Yuan M, Chen J, Bai Y, et al. Unveiling electrochemical urea synthesis by co-activation of CO_2 and N_2 with Mott–Schottky heterostructure catalysts. *Angew Chem Int Ed*. 2021;60(19):10910-10918.
58. Yuan M, Chen J, Xu Y, et al. Highly selective electroreduction of N_2 and CO_2 to urea over artificial frustrated Lewis pairs. *Energy Environ Sci*. 2021;14(12):6605-6615.
59. Mukherjee J, Paul S, Adalder A, et al. Understanding the site-selective electrocatalytic co-reduction mechanism for green urea synthesis using copper phthalocyanine nanotubes. *Adv Funct Mater*. 2022;32(31):2200882.
60. Yuan M, Chen J, Zhang H, et al. Host–guest molecular interaction promoted urea electrosynthesis over a precisely designed conductive metal–organic framework. *Energy Environ Sci*. 2022;15(5):2084-2095.
61. Yuan M, Zhang H, Xu Y, et al. Artificial frustrated Lewis pairs facilitating the electrochemical N_2 and CO_2 conversion to urea. *Chem Catal*. 2022;2(2):309-320.
62. Jiao D, Dong Y, Cui X, et al. Boosting the efficiency of urea synthesis via cooperative electroreduction of N_2 and CO_2 on MoP. *J Mater Chem A*. 2023;11(1):232-240.
63. Lv Z, Zhou S, Zhao L, et al. Coactivation of multiphase reactants for the electrosynthesis of urea. *Adv Energy Mater*. 2023;13(25):2300946.
64. Pan L, Wang J, Lu F, et al. Single-atom or dual-atom in TiO_2 nanosheet: which is the better choice for electrocatalytic urea synthesis? *Angew Chem Int Ed*. 2023;62(8):e202216835.
65. Zhang X, Zhu X, Bo S, et al. Electrocatalytic urea synthesis with 63.5 % Faradaic efficiency and 100 % N-selectivity via one-step C—N coupling. *Angew Chem Int Ed*. 2023;62(33):e202305447.
66. Mei Z, Zhou Y, Lv W, et al. Recent progress in electrocatalytic urea synthesis under ambient conditions. *ACS Sustain Chem Eng*. 2022;10(38):12477-12496.
67. Liu J, Smith SC, Gu Y, Kou L. C—N coupling enabled by N—N bond breaking for electrochemical urea production. *Adv Funct Mater*. 2023;33(47):2305894.
68. Wang Y, Mao J, Meng X, Yu L, Deng D, Bao X. Catalysis with two-dimensional materials confining single atoms: concept, design, and applications. *Chem Rev*. 2019;119(3):1806-1854.
69. Li R, Wang D. Superiority of dual-atom catalysts in electrocatalysis: one step further than single-atom catalysts. *Adv Energy Mater*. 2022;12(9):2103564.
70. Huang JR, Qiu XF, Zhao ZH, et al. Single-product Faradaic efficiency for electrocatalytic of CO_2 to CO at current density larger than 1.2 A cm^{-2} in neutral aqueous solution by a single-atom nanozyme. *Angew Chem Int Ed*. 2022;61(44):e202210985.
71. Li K, Wang Y, Lu J, et al. Screening and mechanistic study of bimetallic catalysts for the electrosynthesis of urea from carbon dioxide and dinitrogen. *Cell Rep Phys Sci*. 2023;4(6):101435.
72. Zhang Z, Xiao J, Chen XJ, et al. Reaction mechanisms of well-defined metal–N_4 sites in electrocatalytic CO_2 reduction. *Angew Chem Int Ed*. 2018;57(50):16339-16342.
73. Wu Y, Jiang Z, Lu X, Liang Y, Wang H. Domino electroreduction of CO_2 to methanol on a molecular catalyst. *Nature*. 2019;575(7784):639-642.
74. Zhong H, Wang M, Ghorbani-Asl M, et al. Boosting the electrocatalytic conversion of nitrogen to ammonia on metal-phthalocyanine-based two-dimensional conjugated covalent organic frameworks. *J Am Chem Soc*. 2021;143(47):19992-20000.
75. Ghorai UK, Paul S, Ghorai B, et al. Scalable production of cobalt phthalocyanine nanotubes: efficient and robust hollow electrocatalyst for ammonia synthesis at room temperature. *ACS Nano*. 2021;15(3):5230-5239.
76. Xu D, Zhang SN, Chen JS, Li XH. Design of the synergistic rectifying interfaces in Mott–Schottky catalysts. *Chem Rev*. 2023;123(1):1-30.
77. Zhang X, Wang Y, Wang Y, et al. Recent advances in electrocatalytic nitrite reduction. *Chem Commun*. 2022;58(17):2777-2787.
78. Shibata M, Yoshida K, Furuya N. Electrochemical synthesis of urea on reduction of carbon dioxide with nitrate and nitrite ions using Cu-loaded gas-diffusion electrode. *J Electroanal Chem*. 1995;387(1):143-145.
79. Feng Y, Yang H, Zhang Y, et al. Te-doped Pd nanocrystal for electrochemical urea production by efficiently coupling carbon dioxide reduction with nitrite reduction. *Nano Lett*. 2020;20(11):8282-8289.
80. Sun H, Yan Z, Liu F, Xu W, Cheng F, Chen J. Self-supported transition-metal-based electrocatalysts for hydrogen and oxygen evolution. *Adv Mater*. 2020;32(3):1806326.
81. Meng N, Huang Y, Liu Y, Yu Y, Zhang B. Electrosynthesis of urea from nitrite and CO_2 over oxygen vacancy-rich ZnO porous nanosheets. *Cell Rep Phys Sci*. 2021;2(3):100378.
82. Abascal E, Gómez-Coma L, Ortiz I, Ortiz A. Global diagnosis of nitrate pollution in groundwater and review of removal technologies. *Sci Total Environ*. 2022;810:152233.
83. Zheng M, Ma H, Li Z, et al. Theoretical insights on C–N coupling mechanism and guidance for screening the catalysts of electrocatalytic urea synthesis by descriptors. *Appl Catal B Environ*. 2024;342:123366.
84. Garcia-Segura S, Lanzarini-Lopes M, Hristovski K, Westerhoff P. Electrocatalytic reduction of nitrate: fundamentals to full-scale water treatment applications. *Appl Catal B Environ*. 2018;236:546-568.
85. Li X, Wu X, Lv X, Wang J, Wu HB. Recent advances in metal-based electrocatalysts with hetero-interfaces for CO_2 reduction reaction. *Chem Catal*. 2022;2(2):262-291.
86. Shin S, Sultan S, Chen ZX, et al. Copper with an atomic-scale spacing for efficient electrocatalytic co-reduction of carbon dioxide and nitrate to urea. *Energy Environ Sci*. 2023;16(5):2003-2013.

87. Qiu M, Zhu X, Bo S, et al. Boosting electrocatalytic urea production via promoting asymmetric C–N coupling. *CCS Chem*. 2023;5(11):2617-2627.
88. Leverett J, Tran-Phu T, Yuwono JA, et al. Tuning the coordination structure of Cu–N–C single atom catalysts for simultaneous electrochemical reduction of CO_2 and NO_3^- to urea. *Adv Energy Mater*. 2022;12(32):2201500.
89. Wang Y, Xia S, Zhang J, et al. Spatial management of CO diffusion on tandem electrode promotes NH_2 intermediate formation for efficient urea electrosynthesis. *ACS Energy Lett*. 2023;8(8):3373-3380.
90. Zhao Y, Ding Y, Li W, et al. Efficient urea electrosynthesis from carbon dioxide and nitrate via alternating Cu–W bimetallic C–N coupling sites. *Nat Commun*. 2023;14(1):4491.
91. Zhang S, Geng J, Zhao Z, et al. High-efficiency electrosynthesis of urea over bacterial cellulose regulated Pd–Cu bimetallic catalyst. *EES Catal*. 2023;1(1):45-53.
92. Meng N, Ma X, Wang C, et al. Oxide-derived core–shell Cu@Zn nanowires for urea electrosynthesis from carbon dioxide and nitrate in water. *ACS Nano*. 2022;16(6):9095-9104.
93. Qin J, Liu N, Chen L, et al. Selective electrochemical urea synthesis from nitrate and CO_2 using in situ Ru anchoring onto a three-dimensional copper electrode. *ACS Sustain Chem Eng*. 2022;10(48):15869-15875.
94. Fu S, Chu K, Guo M, et al. Ultrasonic-assisted hydrothermal synthesis of RhCu alloy nanospheres for electrocatalytic urea production. *Chem Commun*. 2023;59(29):4344-4347.
95. Liu Y, Tu X, Wei X, et al. C-bound or O-bound surface: which one boosts electrocatalytic urea synthesis? *Angew Chem Int Ed*. 2023;62(19):e202300387.
96. Luo Y, Xie K, Ou P, et al. Selective electrochemical synthesis of urea from nitrate and CO_2 via relay catalysis on hybrid catalysts. *Nat Catal*. 2023;6(10):939-948.
97. Sun M, Wu G, Jiang J, et al. Carbon-anchored molybdenum oxide nanoclusters as efficient catalysts for the electrosynthesis of ammonia and urea. *Angew Chem Int Ed*. 2023;62(19):e202301957.
98. Geng J, Ji S, Jin M, et al. Ambient electrosynthesis of urea with nitrate and carbon dioxide over iron-based dual-sites. *Angew Chem Int Ed*. 2023;62(6):e202210958.
99. Lv C, Lee C, Zhong L, et al. A defect engineered electrocatalyst that promotes high-efficiency urea synthesis under ambient conditions. *ACS Nano*. 2022;16(5):8213-8222.
100. Wei X, Wen X, Liu Y, et al. Oxygen vacancy-mediated selective C–N coupling toward electrocatalytic urea synthesis. *J Am Chem Soc*. 2022;144(26):11530-11535.
101. Zhang X, Zhu X, Bo S, et al. Identifying and tailoring C–N coupling site for efficient urea synthesis over diatomic Fe–Ni catalyst. *Nat Commun*. 2022;13(1):5337.
102. Li N, Gao H, Liu Z, et al. Metalphthalocyanine frameworks grown on TiO_2 nanotubes for synergistically and efficiently electrocatalyzing urea production from CO_2 and nitrate. *Sci China Chem*. 2023;66(5):1417-1424.
103. Liu X, Kumar PV, Chen Q, et al. Carbon nanotubes with fluorine-rich surface as metal-free electrocatalyst for effective synthesis of urea from nitrate and CO_2. *Appl Catal B Environ*. 2022;316:121618.
104. Tu X, Zhu X, Bo S, et al. A universal approach for sustainable urea synthesis via intermediate assembly at the electrode/electrolyte interface. *Angew Chem Int Ed*. 2024;63(3):e202317087.
105. Li Y, Zheng S, Liu H, et al. Sequential co-reduction of nitrate and carbon dioxide enables selective urea electrosynthesis. *Nat Commun*. 2024;15(1):176.
106. Wang J, Tan HY, Zhu Y, Chu H, Chen HM. Linking the dynamic chemical state of catalysts with the product profile of electrocatalytic CO_2 reduction. *Angew Chem Int Ed*. 2021;60(32):17254-17267.
107. Li X, Wang S, Li L, Sun Y, Xie Y. Progress and perspective for in situ studies of CO_2 reduction. *J Am Chem Soc*. 2020;142(21):9567-9581.
108. Yang GL, Hsieh CT, Ho YS, et al. Gaseous CO_2 coupling with N-containing intermediates for key C–N bond formation during urea production from coelectrolysis over Cu. *ACS Catal*. 2022;12(18):11494-11504.
109. Zhang Y, Wang Y, Han L, et al. Nitrite electroreduction to ammonia promoted by molecular carbon dioxide with near-unity Faradaic efficiency. *Angew Chem Int Ed*. 2023;62(3):e202213711.
110. Guo M, Fang L, Zhang L, et al. Pulsed electrocatalysis enabling high overall nitrogen fixation performance for atomically dispersed Fe on TiO_2. *Angew Chem Int Ed*. 2023;62(13):e202217635.
111. Zhang S, Wu J, Zheng M, et al. Fe/Cu diatomic catalysts for electrochemical nitrate reduction to ammonia. *Nat Commun*. 2023;14(1):3634.
112. Chen S, Li X, Kao CW, et al. Unveiling the proton-feeding effect in sulfur-doped Fe—N—C single-atom catalyst for enhanced CO_2 electroreduction. *Angew Chem Int Ed*. 2022;61(32):e202206233.
113. Zhang Z, Ma C, Tu Y, et al. Multiscale carbon foam confining single iron atoms for efficient electrocatalytic CO_2 reduction to CO. *Nano Res*. 2019;12(9):2313-2317.
114. Wang H, Jiang Y, Li S, et al. Realizing efficient C–N coupling via electrochemical co-reduction of CO_2 and NO^{3-} on AuPd nanoalloy to form urea: key C–N coupling intermediates. *Appl Catal B Environ*. 2022;318:121819.
115. Liu C, Tong H, Wang P, et al. The asymmetric orbital hybridization in single-atom-dimers for urea synthesis by optimizing the C–N coupling reaction pathway. *Appl Catal B Environ*. 2023;336:122917.
116. Lanigan RM, Sheppard TD. Recent developments in amide synthesis: direct amidation of carboxylic acids and transamidation reactions. *Eur J Org Chem*. 2013;2013(33):7453-7465.
117. Lundberg H, Tinnis F, Selander N, Adolfsson H. Catalytic amide formation from non-activated carboxylic acids and amines. *Chem Soc Rev*. 2014;43(8):2714-2742.
118. Li J, Kornienko N. Electrochemically driven C–N bond formation from CO_2 and ammonia at the triple-phase boundary. *Chem Sci*. 2022;13(14):3957-3964.
119. Kuang S, Xiao T, Chi H, et al. Acetamide electrosynthesis from CO_2 and nitrite in water. *Angew Chem Int Ed*. 2024;63:e202316772.
120. Tao Z, Wu Y, Wu Z, Shang B, Rooney C, Wang H. Cascade electrocatalytic reduction of carbon dioxide and nitrate to ethylamine. *J Energy Chem*. 2022;65:367-370.
121. Rabinowitz JA, Kanan MW. The future of low-temperature carbon dioxide electrolysis depends on solving one basic problem. *Nat Commun*. 2020;11(1):5231.

122. Disch J, Bohn L, Koch S, et al. High-resolution neutron imaging of salt precipitation and water transport in zero-gap CO_2 electrolysis. *Nat Commun*. 2022;13(1):6099.
123. Sassenburg M, Kelly M, Subramanian S, Smith WA, Burdyny T. Zero-gap electrochemical CO_2 reduction cells: challenges and operational strategies for prevention of salt precipitation. *ACS Energy Lett*. 2023;8(1):321-331.
124. Ozden A, Wang Y, Li F, et al. Cascade CO_2 electroreduction enables efficient carbonate-free production of ethylene. *Joule*. 2021;5(3):706-719.
125. Li L, Liu Z, Yu X, Zhong M. Achieving high single-pass carbon conversion efficiencies in durable CO_2 electroreduction in strong acids via electrode structure engineering. *Angew Chem Int Ed*. 2023;62(21):e202300226.
126. Jouny M, Lv JJ, Cheng T, et al. Formation of carbon–nitrogen bonds in carbon monoxide electrolysis. *Nat Chem*. 2019;11(9):846-851.
127. Wang Z, Zhou Y, Liu D, et al. Carbon-confined indium oxides for efficient carbon dioxide reduction in a solid-state electrolyte flow cell. *Angew Chem Int Ed*. 2022;61(21):e202200552.
128. Liu Z, Lv X, Zhang J, et al. Hydroxy-group-enriched In_2O_3 facilitates CO_2 electroreduction to formate at large current densities. *Adv Mater Interfaces*. 2022;9(6):2101956.
129. Ma X, Zhang Y, Fan T, et al. Facet dopant regulation of Cu_2O boosts electrocatalytic CO_2 reduction to formate. *Adv Funct Mater*. 2023;33(16):2213145.
130. Guo C, Zhou W, Lan X, et al. Electrochemical upgrading of formic acid to formamide via coupling nitrite co-reduction. *J Am Chem Soc*. 2022;144(35):16006-16011.
131. Corbin DR, Schwarz S, Sonnichsen GC. Methylamines synthesis: a review. *Catal Today*. 1997;37(2):71-102.
132. Wu Y, Jiang Z, Lin Z, Liang Y, Wang H. Direct electrosynthesis of methylamine from carbon dioxide and nitrate. *Nat Sustain*. 2021;4(8):725-730.
133. Jing H, Long J, Li H, Fu X, Xiao J. Computational insights on electrocatalytic synthesis of methylamine from nitrate and carbon dioxide. *ACS Catal*. 2023;13(15):9925-9935.
134. Bähn S, Imm S, Neubert L, Zhang M, Neumann H, Beller M. The catalytic amination of alcohols. *ChemCatChem*. 2011;3(12):1853-1864.
135. Hayes KS. Industrial processes for manufacturing amines. *Appl Catal A Gen*. 2001;221(1):187-195.
136. Xu L, Tan X, He ZH, et al. Emerging green catalytic synthesis of biomolecules from CO_2 and/or nitrogenous small molecules. *Matter*. 2024;7(1):59-81.
137. Fang Y, Liu X, Liu Z, et al. Synthesis of amino acids by electrocatalytic reduction of CO_2 on chiral Cu surfaces. *Chem*. 2023;9(2):460-471.
138. Wu R, Li F, Cui X, et al. Enzymatic electrosynthesis of glycine from CO_2 and NH_3. *Angew Chem Int Ed*. 2023;62(14):e202218387.
139. Lan J, Wei Z, Lu YR, et al. Efficient electrosynthesis of formamide from carbon monoxide and nitrite on a Ru-dispersed Cu nanocluster catalyst. *Nat Commun*. 2023;14(1):2870.
140. Kim JE, Jang JH, Lee KM, et al. Electrochemical synthesis of glycine from oxalic acid and nitrate. *Angew Chem Int Ed*. 2021;60(40):21943-21951.
141. Jiang N, Zhu Z, Xue W, Xia BY, You B. Emerging electrocatalysts for water oxidation under near-neutral CO_2 reduction conditions. *Adv Mater*. 2022;34(2):2105852.
142. Yan D, Mebrahtu C, Wang S, Palkovits R. Innovative electrochemical strategies for hydrogen production: from electricity input to electricity output. *Angew Chem Int Ed*. 2023;62(16):e202214333.
143. Yamaguchi K, Kobayashi H, Oishi T, Mizuno N. Heterogeneously catalyzed synthesis of primary amides directly from primary alcohols and aqueous ammonia. *Angew Chem Int Ed*. 2012;51(2):544-547.
144. Meng N, Shao J, Li H, et al. Electrosynthesis of formamide from methanol and ammonia under ambient conditions. *Nat Commun*. 2022;13(1):5452.
145. Shao J, Meng N, Wang Y, et al. Scalable electrosynthesis of formamide through C−N coupling at the industrially relevant current density of 120 mA cm^{-2}. *Angew Chem Int Ed*. 2022;61(44):e202213009.
146. Lu Y, Li Y, Zhou B, et al. Anodic electrosynthesis of amide from alcohol and ammonia. *CCS Chem*. 2024;6(1):125-136.
147. Zhao S, Yang Y, Tang Z. Insight into structural evolution, active sites, and stability of heterogeneous electrocatalysts. *Angew Chem Int Ed*. 2022;61(11):e202110186.
148. Lai W, Ma Z, Zhang J, Yuan Y, Qiao Y, Huang H. Dynamic evolution of active sites in electrocatalytic CO_2 reduction reaction: fundamental understanding and recent progress. *Adv Funct Mater*. 2022;32(16):2111193.
149. Xu Y, Yang H, Chang X, Xu B. Introduction to electrocatalytic kinetics. *Acta Phys-Chim Sin*. 2022;39:2210025.
150. Yuan T, Voznyy O. Guidelines for reliable urea detection in electrocatalysis. *Cell Rep Phys Sci*. 2023;4(8):101521.

How to cite this article: Zhang Z, Li D, Tu Y, et al. Electrocatalytic synthesis of C–N coupling compounds from CO_2 and nitrogenous species. *SusMat*. 2024;4:e193. https://doi.org/10.1002/sus2.193

AUTHOR BIOGRAPHIES

Zheng Zhang received his PhD degree in physical chemistry from Xiamen University in 2020. He was then a postdoctoral research fellow at Department of Physical Chemistry and Materials Science, University of Szeged. In 2022, he joined College of Chemistry and Chemical Engineering at Wuhan Textile University. He was awarded by the "Wuhan Talent Plan" in 2023. His current research interests mainly focus on the development of new catalysts for electrocatalytic conversion of C_1 molecules, and the in-depth understanding of electrocatalytic mechanisms.

Junjiang Zhu received his PhD degree in Changchun Institute of Applied Chemistry, Chinese Academy of Sciences in 2005. From 2005 to 2018, he has worked at Fuzhou University, University of Porto, Technical University of Berlin, South-Central Minzu University and Shenyang Normal University, as a full faculty or a postdoctoral researcher. At the end of 2018, he joined Wuhan Textile University as a Distinguished professor of "Chutian Scholars" of Hubei province. He was honored to be in the "Top 2% of the world's top scientists list" in 2023. He has authored over 90 papers with total citations over 4000 and an H-index of 27. His current research mainly focuses on rational design of perovskite oxides and carbonaceous materials and their applications in environmental and energy catalysis.

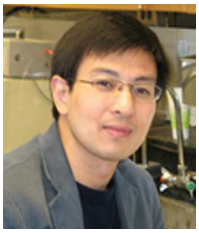

Xuping Sun received his PhD degree in Changchun Institute of Applied Chemistry (CIAC), Chinese Academy of Sciences in 2006. During 2006–2009, he carried out postdoctoral researches at Konstanz University, University of Toronto, and Purdue University. In 2010, he started his independent research career as a Full Professor at CIAC and then moved to Sichuan University in 2015. In 2018, he joined University of Electronic Science and Technology of China. He was recognized as a highly cited researcher in both areas of chemistry and materials science by Clarivate Analytics. He published over 700 papers with total citations over 74 000 and an H-index of 143. His current research mainly focuses on rational design of functional nanomaterials toward applications in catalysis, sensing, and biomedicine.